RIG-I and PKR, but not stress granules, mediate the pro-inflammatory response to Yellow fever virus

Guillaume Beauclair[1], Felix Streicher[1], Daniela Bruni[1], Ségolène Gracias[1], Salomé Bourgeau[1], Laura Sinigaglia[1], Takashi Fujita[2], Eliane F. Meurs[1], Frédéric Tangy[1] and Nolwenn Jouvenet[1]*

[1] *Viral Genomics and Vaccination Unit, Institut Pasteur, UMR3569 CNRS, 75015 Paris, France*

[2] *Department of Virus Research, Institute for Frontier Life and Medical Sciences, Kyoto University, Kyoto, Japan.*

Short title: Innate response against YFV in liver cells

*Corresponding author: nolwenn.jouvenet@pasteur.fr

Abstract

Yellow fever virus (YFV) is a single-stranded RNA virus primarily targeting the liver. Severe YF cases are responsible for viral hemorrhagic fever, plausibly precipitated by excessive pro-inflammatory cytokine response, resulting in up to 50% fatality. Pathogen recognition receptors (PRRs), such as the ubiquitously expressed cytoplasmic RIG-I-like receptors (RLRs), as well as the viral RNA sensor PKR are known to initiate a pro-inflammatory response upon recognition of viral genomes and replication intermediates. The PRRs responsible for cytokine production in cells infected with YFV strains are not known.

Here, we sought to reveal the main determinants responsible for the acute cytokine expression occurring in human hepatocytes following YFV infection. Using a RIG-I-defective human hepatoma cell line, we found that RIG-I largely contributes to cytokine secretion upon infection with the Asibi strain. In infected RIG-I-proficient hepatoma cells, RIG-I was localized in stress granules. These granules are large aggregates of stalled translation preinitiation complexes known to concentrate RLRs and PKR, and are so far recognized as hubs orchestrating RNA virus sensing. Using PKR-deficient hepatoma cells, we found that PKR contributes to both stress granule formation and cytokine induction upon Asibi infection. However, we showed that stress granules disruption did not affect the cytokine response to Asibi infection, as assessed by siRNA-knockdown-mediated inhibition of stress granule assembly and an automated determination of granule size and number. Finally, no viral RNA was detected in stress granules using a fluorescence *in situ* hybridization approach coupled with immunofluorescence.

Collectively, our data strongly suggest that both RIG-I and PKR mediate pro-inflammatory cytokine induction in YFV-infected hepatocytes, in a stress granule-independent manner. Therefore, by showing the uncoupling of the early cytokine response from the stress granules formation, our model challenges the current view by which stress granules are required for the mounting of the acute antiviral response.

Author Summary

Yellow fever is a mosquito-borne acute hemorrhagic disease caused by yellow fever virus (YFV). The mechanisms responsible for its pathogenesis remain largely unknown, although increased inflammation has been linked to worsened outcome. In the early phases of infection, YFV targets the liver, where it primarily infects hepatocytes. Pathogen-recognition receptors (PRRs) are the first immune sensors detecting microbial infections. The PRR(s) responsible for the recognition of the YFV in human hepatocytes remains to be established. Here, we first show that YFV's sensing by two PRRs, RIG-I and PKR, elicits the induction and production of pro-inflammatory mediators in human hepatocytes. We show that YFV infection promotes the formation of cytoplasmic structures, termed stress granules, in a PKR-, but not RIG-I-dependent manner, and that these structures are dispensable for downstream signaling via these receptors. Whilst stress granules were previously postulated to be essential platforms for PRRs activation, here we first uncovered that they are not required for pro-inflammatory mediators' production upon YFV infection. Collectively, our work uncovered the molecular events triggered by YFV, which could prove instrumental in clarifying the pathogenesis of the disease, with possible repercussions on disease management.

Introduction

Flaviviruses are a group of more than seventy enveloped RNA viruses that can cause serious diseases in humans and animals [1,2]. They have provided some of the most important examples of emerging or resurging diseases of global significance. Most flaviviruses, such as dengue virus (DENV), yellow fever virus (YFV) and Zika virus (ZIKV), are arthropod-borne viruses transmitted to vertebrate hosts by mosquitoes or ticks [1]. YFV is the prototype and eponymous virus of the Flavivirus genus. It is a small (40–60 nm), enveloped virus harboring a single positive-strand RNA genome of 11 kb. The genome encodes a polyprotein that is cleaved co- and post-translationally into three structural proteins: capsid (C), membrane precursor (prM) and envelope (E), and seven non-structural (NS) proteins (NS1, NS2a, NS2b, NS3, NS4a, NS4b, and NS5). The C, prM, and E proteins are incorporated into the virions, while

80 NS proteins are found only in infected cells [3]. NS proteins coordinate RNA replication, viral assembly
81 and modulate innate immune responses, while the structural proteins constitute the virion.
82 YFV is endemic in the tropical regions of sub-Saharan Africa and South America. The reference
83 strain Asibi was isolated in 1927 in West Africa from the blood of a human patient. The vaccine strain
84 17D was developed empirically in the 1930s, by passaging the Asibi strain in rhesus macaques, mouse
85 and chicken embryonic tissues [4]. 17D is one of the most effective vaccines ever generated. It has been
86 used safely and effectively on more than 600 million individuals over the past 70 years [4]. However,
87 due to poor vaccine coverage and vaccine shortages, the virus continues to cause disease in endemic areas,
88 as illustrated by recent outbreaks in Angola and Brazil [5,6].
89 Yellow fever (YF) pathogenesis is viscerotropic in humans, with viral replication in the liver critical
90 to the establishment of the disease [3]. Severe YF is responsible for multi-system organ failure and viral
91 hemorrhagic fever resulting in up to 50% fatality. Similar to Ebola hemorrhagic fever, cytokine dysregulation
92 is thought to result in endothelial damage, disseminated intravascular coagulation and circulatory shock
93 observed in the terminal stage of the disease. Viral hemorrhagic fever is considered as an illness
94 precipitated by excessive pro-inflammatory cytokine response ('cytokine storm') [7,8]. Almost any cell
95 type in the body can produce pro-inflammatory cytokines in response to various stimuli, such as a viral
96 infection [9]. The pattern of cytokine expression in response to infection with pathogenic strains of YFV
97 has been described both in humans and in rhesus macaques. Studies performed on patients during a YF
98 outbreak in the Republic of Guinea in 2000 showed that excessive production of pro-inflammatory
99 cytokines, such as IL6 and TNFα, correlates with high viremia and disease outcome [10]. The levels of
100 these two cytokines were statistically higher in patients with fatal hemorrhagic fever than in patients
101 who survived. Similar findings were obtained with rhesus macaques infected with the strain Dakar-
102 HD1279 [11]. The animals died of hemorrhagic fever within five days. These studies also suggest that
103 pro-inflammatory cytokines might be produced by injured organs, especially the liver, and not by cells
104 circulating in the blood [11].
105 Upon viral infection, the cytokine response is initiated by the recognition of viral genomes and viral
106 replication intermediates by pathogen recognition receptors (PRRs) [12], such as the ubiquitously
107 expressed cytoplasmic RIG-I-like receptors (RLRs). Three RLRs have been identified in vertebrates:

108 melanoma differentiation-associated gene 5 (MDA5), laboratory of genetics and physiology 2 (LGP2)
109 and retinoic acid inducible gene 1 (RIG-I) [13]. Upon binding to viral nucleic acids, MDA5 and RIG-I
110 undergo a conformational change, which allows interaction with the adaptor protein MAVS and
111 subsequent recruitment of signaling complexes that comprises protein kinases such as TBK1, IKKα,
112 IKKβ and IKKε [14]. These events lead to the activation and nuclear translocation of the transcription
113 factors IRF3 and NF-κB, which stimulate the rapid expression of pro-inflammatory cytokines and type
114 I interferons (IFNs).

115 RIG-I plays an important role in initiating the IFN-mediated antiviral response against DENV and
116 ZIKV [15–18]. Induction of cytokines upon infection with the vaccine strain of YFV is also mediated
117 by RIG-I in plasmacytoid dendritic cells [19]. Whether RIG-I contributes to cytokine production in cells
118 infected with wild-type YFV strains is not known.

119 The subcellular localization where RIG-I interacts with its ligands is not well described. Upon
120 infection with influenza A virus lacking its non-structural protein 1 (IAVΔNS1), Newcastle disease
121 virus or Sendai virus [20–23], RIG-I accumulates in cytoplasmic foci. Disruption of these foci, which
122 have been identified as stress granules, reduced the abundance of *IFNB* mRNAs in IAVΔNS1-infected
123 cells [20]. Thus, stress granules may be important for RIG-I signaling and could serve as a platform for
124 viral RNA sensing. Moreover, other viral nucleic sensors, such as MDA5 [24], LGP2 [25] and cGAS
125 [26], are also concentrated in stress granules. Finally, numerous viruses interfere with stress granule
126 formation, *via*, for instance, the cleavage of one of their core components by a viral protease. Thus,
127 accumulation of viral sensors in stress granules and viral counteraction mechanisms suggest that these
128 granules act as hubs that coordinate foreign nucleic acid sensing [27,28].

129 Stress granules are non-membranous cytoplasmic structures that concentrate translationally stalled
130 mRNAs and proteins [29]. Their assembly is triggered by sensing distinct types of stress, including viral
131 infection, by one of four kinases, resulting in phosphorylation of the eukaryotic initiation factor 2α
132 (eIF2α). These kinases are: the heme-regulated inhibitor (HRI), which is activated by heat shock or
133 oxidative stress (*e.g.* by reactive oxygen species (ROS) produced upon treatment with sodium arsenite);
134 general control non-depressible protein 2 (GCN2), which reacts to UV-induced damage or amino acid
135 deprivation; dsRNA-sensing protein kinase R (PKR); and PKR-like endoplasmatic reticulum (ER)

136 kinase (PERK), which is activated upon ER stress [29]. Stress granule assembly does not only arrest the
137 host translation machinery, but also heavily disturb viral translation, which is further evidence for their
138 antiviral nature [27,28,30]. Here, we investigated the role of RIG-I, PKR and stress granules in the
139 induction inflammatory cytokines upon infection of hepatoma cells with YFV.
140
141
142 **Results**
143 **The Asibi strain of YFV triggers the production of pro-inflammatory cytokines in hepatoma cells**
144 **through RIG-I, IRF3 and NF-κB**
145 We examined whether the YFV reference strain Asibi could trigger the expression of pro-
146 inflammatory cytokines in human hepatoma cells through the RIG-I signaling pathway. Huh7 and
147 Huh7.5 cells, a clone derived from Huh7 that expresses an inactive form of the viral sensor RIG-I [31],
148 were infected with the Asibi strain for 24 or 48 hours. The abundances of *TNFA*, *IL6* and *IFNB* mRNAs
149 increased over time with infection in Huh7 cells, while being significantly lower in Huh7.5 cells at 48
150 hours post-infection (hpi) (**Fig 1A-C**). Addition of BAY11-7085 (BAY), an irreversible inhibitor of
151 IκBα phosphorylation that prevents activation of NF-κB [32], reduced induction of *TNFA*, *IL6* and *IFNB*
152 mRNAs in Huh7 cells infected with Asibi (**Fig 1A-C**). However, the mRNA levels of these three
153 cytokines in BAY-treated Huh7 cells were higher compared to those in Huh7.5 cells (**Fig 1A-C)**.
154 Infection of the Huh7 cells, either treated with BAY or left untreated, produced similar amounts of viral
155 RNA (**Fig 1D)**, which suggests that the chemical treatment did not affect viral replication. Furthermore,
156 we noticed that Huh7.5 cells infected for 48 hours produced approximately three-fold more viral RNA
157 than Huh7 cells infected for the same amount of time (**Fig 1D)**, suggesting that absence of RIG-I
158 signaling favors viral replication. Untreated Huh7 cells secreted around 10 to 20 pg/ml of IL6 and TNFα
159 protein after 48 hours of infection, but not after 24 hpi (**Fig 1E, F**). By contrast, the amount of IL6 and
160 TNFα protein secreted by cells treated with the inhibitor of IκBα phosphorylation or expressing the
161 inactive form of RIG-I was below the detection limit of the ELISA (**Fig 1E, F**). Together, these data
162 suggest that Asibi infection triggers the induction and secretion of pro-inflammatory cytokines in a RIG-
163 I- and NF-κB- dependent manner in human hepatoma cells.

164 By Western blot analysis, we found that IRF3 was activated in Huh7 cells infected with Asibi for
165 24 or 48 hours, but not in non-infected cells (**Fig 1G**). The level of IRF3 phosphorylation was higher at
166 48 than at 24 hpi, despite the total protein abundance being similar at these two points in time (**Fig 1G**).
167 IRF3 was not phosphorylated in Huh7.5 cells infected with Asibi (**Fig 1G**). In Huh7 cells treated with
168 BAY, IRF3 was not phosphorylated at 24 hpi (**Fig 1G**). Phosphorylation was present at 48 hpi, tough in
169 small levels than in non-treated cells (**Fig 1G**). IκBα is a negative regulator of the NF-κB pathway: its
170 degradation triggers the nuclear translocation of the NF-κB subunits p65 and p50. IκBα was degraded
171 in Huh7 cells infected for 48 hours but less so in cells treated with BAY for 48 hours (**Fig 1G**). Slightly
172 more of the viral protein NS4b was produced in Huh7.5 cells than in Huh7 cells upon 48 hours of Asibi
173 infection (**Fig 1G**), which is consistent with the RT-qPCR analysis (**Fig 1D**). These experiments indicate
174 that both IRF3 and NF-κB are activated during Asibi infection of human hepatoma cells and that RIG-
175 I contributes to IRF3 activation.
176 Immunofluorescence analysis revealed that IRF3 was detectable exclusively in the cytosol of 100%
177 of uninfected cells, whereas it was found both in the cytosol and the nucleus of around 50% of cells
178 infected for 24 hours (**Fig 1H**). Infected cells were identified with antibodies recognizing dsRNA
179 structures, including probably viral replicative intermediates (**Fig 1H**). Similar quantification showed
180 that around 3% of uninfected cells exhibited nuclei positive for the NF-κB subunit p65 whereas around
181 65% of Asibi-infected cells showed nuclei positive for p65 (**Fig 1I**).
182 Together, these results suggest that both the NF-κB and the IRF3 pathways are involved in cytokine
183 secretion in human hepatoma cells upon Asibi infection and that their initiation is dependent on RIG-I.
184
185 **RIG-I localizes in stress granules in human and monkey cells infected with YFV**
186 Having determined that RIG-I is important for mediating a cytokine response in Huh7 cells infected
187 with Asibi (**Fig 1**), we then investigated its subcellular localization. The distribution of the RIG-I signal
188 was found to be weak and diffuse in the cytosol of uninfected Huh7 cells (**Fig 2A**), which is consistent
189 with data reported for unstimulated HeLa cells [20]. After infection with Asibi for 24 hours, RIG-I
190 accumulated in cytosolic foci (**Fig 2A**). Since RIG-I was previously shown to localize in stress granules

191 in HeLa cells infected with several types of viruses [20–23], the Huh7 cells were also stained with the
192 stress granule marker TIA-1 related protein (TIAR). In non-infected cells, the TIAR signal was weak
193 and diffused in the cytoplasm and in the nucleus of the cells. In infected cells, TIAR was redistributed
194 into cytoplasmic foci (**Fig 2A**). The RIG-I structures present in infected cells co-localized with TIAR
195 foci (**Fig 2A**, zoom images for details), suggesting that RIG-I is recruited to stress granules upon
196 infection. The intensity profiles of individual foci confirmed that the RIG-I signal and the TIAR signal
197 overlapped (**Fig 2A**, right panels). These profiles also revealed that dsRNAs seemed to be excluded
198 from stress granules (**Fig 2A**).

199 To follow the formation of stress granules in infected cells, the localization of TIAR and RAS
200 GTPase-activating protein SH3 domain-binding protein 1 and 2 (G3BP), which are canonical stress
201 granule markers [33], were examined in Huh7 cells infected with Asibi for over time (**Fig 2B**). Infected
202 cells were identified by the presence of the viral protein NS4b (**Fig 2B**). TIAR and G3BP were diffuse
203 in non-infected cells. They remained diffuse until 12 hpi, where 16% of cells were determined positive
204 for NS4b. Fifteen hours after infection, around 80% of cells were infected and around 40% of the total
205 number of cells exhibited TIAR- and G3BP-positive foci (**Fig 2B**). At 24 hpi, all cells were infected and
206 around 70% of them were positive for TIAR- and G3BP- containing foci. At 37 hpi, all cells remained
207 infected and around 20% of them exhibited TIAR- and G3BP positive foci. These foci resembled the
208 ones detected in Huh7 cells treated with sodium arsenite (NaArs), a chemical commonly used for
209 induction of oxidative stress in eukaryotic cells, for 30 minutes (**Fig 2B**). These results indicate that
210 upon Asibi infection, TIAR- and G3BP- positive foci appeared between 12 and 15 hpi, peak around 24
211 hpi and persist in around 20% of cells until later times. Moreover, these data suggest that the formation
212 of the stress granules occur throughout infection with Asibi.

213 To further validate the nature of the TIAR- and G3BP- positive foci observed in infected cells, we
214 assessed their sensitivity to cycloheximide. Cycloheximide is a compound that inhibits stress granule
215 formation and fosters their disassembly by stabilizing mRNAs on polysomes [34]. Huh7 cells treated
216 with NaArs for 30 min and subsequently incubated with cycloheximide for 1 hour or left untreated were
217 used as positive controls (**Fig 2C**). Alternatively, cells were infected with Asibi for 48 hours and then
218 treated, or not, with cycloheximide for 1 hour. The TIAR and the G3BP signals overlapped, both in cells

219 infected by Asibi for 48 hours and in NaArs-treated cells (**Fig 2C**). Cycloheximide treatment led to a
220 complete loss of TIAR- and G3BP- positive foci, both in NaArs -treated cells and in Asibi-infected cells
221 (**Fig 2C**, compare non-treated and treated cells). These results suggest that, under both conditions, most
222 mRNAs trapped in these cytoplasmic foci can be released within 1 hour and undergo some translation
223 on polysomes. Most importantly, these experiments confirmed that the cytoplasmic foci containing
224 TIAR, G3BP and RIG-I identified in infected cells also contained mRNAs, and as such, can be defined
225 as canonical stress granules. Furthermore, these experiments also showed that the stress granule proteins
226 TIAR and G3BP are not recruited to Asibi replication complexes identified by NS4b,in contrast to
227 observations reported for ZIKV, DENV and WNV [35,36].

228 We next monitored the formation of stress granules upon Asibi infection in different cell models
229 than Huh7. Like Huh7 cells, HepG2 cells are hepatocyte-derived cells and are thus relevant for infection
230 with YFV, a hepatotropic virus. TIAR- and G3BP-positive foci were detected in HepG2 cells infected
231 for 48 hours (**Fig 3A**). Stress granules were also detected in CMMT cells, a *Macaca mulatta* epithelial
232 cell line, upon 24 hours of infection with Asibi (**Fig 3B**). Macaques are natural hosts of YFV during the
233 jungle cycle of transmission [37]. Similarly, TIAR- and G3BP-positive foci were observed in Huh7 cells
234 infected with the clinical isolate HD1279 (HD Dakar) for 24 hours (**Fig 3C**). These data indicate that
235 infection with two YFV strains triggers the formation of stress granules in several mammalian cell lines,
236 suggesting that the stress response is neither viral strain nor cell type specific.

237

238 **PKR contributes to stress granule formation and innate response in Asibi-infected Huh7 cells**

239 PKR is known to be activated upon infection with several flaviviruses, including ZIKV, WNV and
240 Japanese Encephalitis virus (JEV) [38–40] and to play an important role in stress granule nucleation
241 through its ability to phosphorylate the eukaryotic initiation factor eIF2α [41]. We first assessed whether
242 PKR was activated upon Asibi infection of Huh7 cells. Western blot analysis showed that PKR was
243 phosphorylated in Huh7 cells infected for 24 and 48 hours, but not in non-infected cells (**Fig 4A**). Thus,
244 PKR is activated upon Asibi infection of Huh7 cells. To evaluate the role of PKR in the formation of
245 stress granules in Asibi-infected human hepatic cells, we generated a Huh7 short hairpin (sh)-PKR cell
246 line by transduction with lentiviruses expressing short hairpin RNAs (shRNAs) specific for PKR. While

247 PKR expression was detectable in Huh7 cells transduced with lentivirus expressing control shRNA
248 targeting luciferase (Huh7-shLuc cells), it was not detectable in Huh7-shPKR cells (**Fig 4B**). As a
249 control experiment, we treated the cells with NaArs, which induces stress granule formation *via* HRI-
250 mediated eIF2α phosphorylation [42]. TIAR- and G3BP- positive stress granules were detected in both
251 Huh7-shLuc and Huh7-shPKR cells treated with NaArs for 30 minutes (**Fig 3C**). This confirms that the
252 absence of PKR does not disrupt the formation of NaArs-dependent stress granule induction.

253 Automated microscopic quantification revealed that around 10% of Huh7-shLuc cells infected at a
254 MOI of 2 for 24 or 34 hours contained at least two stress granules (**Fig 4 D-E**). At a MOI of 20, around
255 25% of Huh7-shLuc cells were positive for stress granules at 24 and 34 hpi (**Fig 4 D-E)**. No TIAR- nor
256 G3BP- positive foci were detected in Huh7-shPKR cells infected at a MOI of 2 for 24 or 34 hours. At a
257 MOI of 20, a low percentage (around 1%) of Huh7-shPKR cells exhibited detectable stress granules
258 (**Fig 4 D-E)**. These stress granules possibly formed in a PKR-independent manner, *via* the activation of
259 other members of the eIF2α kinase family. Alternatively, a minute quantity of PKR still being expressed
260 in shPKR cells may initiate the formation of these granules. A similar proportion of Huh7-shLuc and
261 Huh7-shPKR cells were found positive for NS4b at 24 or 34 hpi at the two tested MOIs (**Fig 4F**).
262 Together, we conclude that PKR plays a key role in stress granule formation in Asibi-infected human
263 hepatic cells and that the absence of stress granules has no effect on viral infection.

264 We next tested whether other members of the eIF2α kinase family are involved in stress granule
265 formation in Huh7 cells infected with Asibi. Therefore, cells infected for 24 hours were treated for four
266 hours with either GSK2606414 (GSK) or GCN2-IN-1 (iGCN2), which are inhibitors of PERK [43] and
267 GCN2, respectively. Around 78% of control DMSO-treated cells were positive for TIAR- and G3BP-
268 foci at 24 hpi (**Fig 5**). Only 2% and 4% of GSK- and iGCN2- treated cells, respectively, exhibited stress
269 granules (**Fig 5**), indicating that both inhibitors suppressed Asibi-induced stress granule formation.
270 These data suggest that at least three of the four eIF2α kinases (GCN2, PERK and PKR) contribute to
271 stress granule formation in human hepatoma cells infected with Asibi. Thus, Asibi infection induces an
272 integrated stress response in Huh7 cells.

273 Since no stress granules were detected in cells depleted of PKR in three of four conditions tested
274 (**Fig 4E**), we used Huh7-shPKR cells to determine whether absence of granules affected cytokine

275 induction. Consistent with our Western blot data (**Fig 4B**), RT-qPCR analysis showed that *PKR* mRNAs
276 abundance was reduced by more than 90% in Huh7-shPKR cells in comparison to Huh7-shLuc cells
277 **(Fig 6A**). These RT-qPCR analyses also showed that the viral RNA yield in Huh7-shPKR cells was not
278 markedly different from that in Huh7-shLuc cells 24 hours or 34 hours after infection either at a MOI
279 of 2 or 20 (**Fig 6B**), which is consistent with our microscopic analysis (**Fig 4F**). *IL6* mRNA abundance
280 was significantly lower in Huh7-shPKR cells than that of Huh7-shLuc when cells were infected at a
281 MOI of 20 (**Fig 6C).** The abundances of *TNFA* and *IFNB* mRNAs were significantly lower in Huh7-
282 shPKR cells than those in infected Huh7-shLuc under the same conditions of infection **(Fig 6D-E**). This
283 is consistent with our preceding observation of cytokine induction in Asibi infected cells being
284 dependent on NF-κB (**Fig 1**) and with a previous report showing that PKR is involved in the induction
285 of the *IFN* through the activation of NF-κB [44]. Thus, at least two nucleic acid sensors, namely RIG-I
286 (**Fig 1**) and PKR (**Fig 4**), contribute to the antiviral response against Asibi in Huh7 cells.
287 Taken together, our data show that PKR contributes to both stress granule formation and induction
288 of cytokines in Huh7 cells infected with Asibi. However, since PKR does not require its kinase activity
289 to stimulate NF-κB [44,45], it might contribute to the cytokine induction in Asibi-infected cells in a
290 eIF2α- (and thus stress granule-) independent manner.
291
292 **Inhibition of stress granule formation has a limited effect on antiviral response**
293 To further investigate the putative link between stress granules and the induction of antiviral
294 cytokines, we used a siRNA-knockdown approach to inhibit stress granule assembly. We tested
295 numerous combinations of siRNAs targeting core granule components in infected cells. The most
296 efficient strategy consisted in transfecting Huh7 cells twice with four pools of siRNAs targeting TIAR,
297 TIA-1, G3BP1 and G3BP2 (siSG). In these cells, we monitored stress granule formation using
298 antibodies against eIF3b and eIF4G, two core components of stress granules. Around 30% of Huh7 cells
299 transfected with scrambled control siRNAs and infected at a MOI of 2 or 20 for 24 hours contained at
300 least two eIF4G- and eIF3b-positive foci (**Fig 7 A-B**). When cells were transfected with the 4 siRNA
301 pools and infected under the same conditions and for the same amount of time, less than 5% of cells

302 exhibited stress granules (**Fig 7 A-B**). The impact of the siRNA against TIAR, TIA-1, G3BP1 and
303 G3BP2 on the number of cells positive for stress granules following 34 hours of infection was also
304 significant at the two tested MOIs (**Fig 7B**). Under the four tested conditions, the surface area occupied
305 by stress granules per cell was significantly reduced in cells transfected with the mixture of four siRNA
306 pools compared to the controls (**Fig 7C**). These experiments validate our silencing approach as an
307 efficient way to significantly reduce both the number of cells positive for stress granules and the surface
308 occupied by stress granules per cell. Transfection with the 4 siRNA pools had no effect on viral
309 infection, when compared to transfection with control siRNAs **(Fig 7D)**. RT-qPCR analysis showed that
310 TIAR, TIA-1, G3BP1 and G3BP2 mRNA abundances were significantly reduced in cells transfected
311 with the 4 siRNA pools as compared to cells transfected with control siRNAs **(Fig 8 A-D)**. Of note,
312 TIAR and TIA-1 expression was induced three- to four-fold by infection, in an MOI-dependent
313 response. This may be a consequence of virally-induced stress. Transfection of the four siRNA pools
314 has no effect on *TNFA, IL6* and *IFNB* mRNA abundances nor on viral RNA yield **(Fig 8 E-H)**. Together,
315 these data show that significant reduction of stress granule numbers and size did not suppress the
316 cytokine response to Asibi infection. Thus, in our model, stress granules have a limited contribution to
317 the initiation of the antiviral response.
318
319 **RIG-I signaling is not involved in stress granule assembly**
320 In Huh7 cells, RIG-I signaling is crucial for cytokine induction and secretion upon Asibi infection
321 (**Fig 1**). Therefore, we wondered whether RIG-I signaling would participate in stress granule assembly
322 and/or maintenance. We quantified the proportion of Huh7 and Huh7.5 cells that were positive for stress
323 granules at 24 and 34 hpi following infection at two MOIs. A similar proportion of Huh7 and Huh7.5
324 cells were found positive for stress granule markers in all tested conditions (**Fig 9 A-B**). No difference
325 in the number of cells positive for NS4b was observed between Huh7 and Huh7.5 cells (**Fig 9C**). We
326 conclude that the absence of RIG-I signaling had no effect on the number of granules that assemble in
327 response to infection. It is thus unlikely that RIG-I mediates a feed-forward loop to maintain stress
328 granule assembly.
329

330 **YFV RNA is excluded from stress granules**

331 Our previous analysis showed that neither dsRNA (**Fig 2A**) nor the viral proteins NS4b and NS1
332 (**Fig 2B, 3, 4D, 5, 7A** and **9A**) seem to be recruited to stress granules. To further investigate the putative
333 association between stress granules containing RIG-I (**Fig 2A**) and viral RNA, we used an RNA
334 fluorescence *in situ* hybridization (FISH) approach coupled with immunofluorescence and confocal
335 microscopy. The Asibi-specific FISH probe produced no signal in non-infected Huh7 control cells (**Fig**
336 **10A**) and a bright punctate signal in the cytoplasm of infected cells (**Fig 10A**), confirming the specificity
337 of the probe [46]. Asibi RNA was never found to be associated with TIAR-foci (**Fig 10A,** enlarged
338 panels). This was unexpected since RIG-I signaling is key to cytokine induction and production (**Fig.1**)
339 and massively concentrate in stress granules in Asibi-infected cells (**Fig 2A**). These results suggest that
340 an interaction between viral RNA and RIG-I might not happen in stress granules in Asibi-infected Huh7
341 cells. A minute quantity of RIG-I might however interact with viral RNA in ER-derived replication sites
342 and initiates a stress granule-independent IFN response. In line with this, RIG-I was recruited to TIAR-
343 positive granules in Huh7 cells treated with NaArs (**Fig 10B**), which is consistent with previous
344 observations on NaArs-treated HeLa cells [20]. These data further indicate that RIG-I recruitment to
345 stress granules can occur in absence of viral RNA.

346

347 **Discussion**

348 The identity of the PRR(s) responsible for the initiation of a pro-inflammatory response upon direct
349 infection of human hepatocytes with the wild-type strain of YFV has not been uncovered thus far. In
350 this study, we first identified RIG-I and PKR as main actors responsible for the induction and production
351 of pro-inflammatory cytokines upon infection of human hepatocytes with the Asibi strain of YFV. We
352 demonstrated the crucial involvement of RIG-I in this process by directly comparing the dysfunctional
353 RIG-I-expressing human hepatoma cell line Huh7.5. with its RIG-I -competent counterpart (Huh7 cells).
354 The level of IL6 and TNFα secreted in the first 48 hours of infection by Huh7.5 cells upon Asibi
355 infection was under the limit of detection, whilst both cytokines were produced in Huh7 cells in the
356 same experimental conditions. This is in accordance with our previous studies showing that human
357 plasmacytoid dendritic cells infected with the YFV vaccine strain 17D induced an IFN response in a

358 RIG-I dependent manner [19]. Furthermore, the increased viral load found in the absence of a functional
359 RIG-I demonstrates the direct anti-viral role of the effector mechanisms initiated by this sensor. Other
360 members of the RLR family may contribute to YFV sensing in other cell types or at later time of
361 infection. Such distinct temporal activity of RIG-I and MDA5 during infection with the related West
362 Nile Virus has been reported in mice [47].

363 In Huh7 cells silenced for PKR and infected with Asibi, cytokine expression was, in most of the
364 tested conditions, below the detection limit. This suggests that PKR, like RIG-I, largely contributes to
365 the initiation of the antiviral response. This is consistent with the previously reported role of PKR in the
366 production of IFN and other pro-inflammatory cytokines upon viral infection, possibly *via* its interaction
367 with the IKK complex and subsequent activation of NF-κB [44,48]. Moreover, PKR was previously
368 described as an important effector protein against infection with WNV in mice [40].

369 The fact that abolishing RIG-I signaling or silencing PKR drastically reduces the pro-inflammatory
370 response in Asibi infected cells shows the non-redundant nature of these two dsRNA sensors in
371 maintaining cytokine production. We speculate that RIG-I and PKR cooperate to induce an anti-YFV
372 response. Indeed, PKR interacts with RIG-I and MDA5 in HEK293T cells transfected with FLAG-
373 tagged versions of RIG-I or MDA5 and infected with a mutant vaccinia virus lacking a gene known to
374 inhibit PKR [49]. However, in this context, PKR was only required for MDA5, but not RIG-I mediated,
375 IFN production [49]. Consistent with the hypothesis that PKR and RIG-I cooperate to orchestrate
376 antiviral response, PKR is known to interact with several members of the TRAF family, including
377 TRAF2 and TRAF6 [50,51], two proteins involved in MAVS signaling. Finally, MAVS, which acts
378 downstream of RIG-I and MDA5, interacts with PKR [52] and is essential for PKR-induced IFN
379 production [49].

380 Stress granules have been demonstrated to contain and concentrate viral nucleic sensors; hence,
381 they are generally regarded as a functional platform for ligand recognition and subsequent induction of
382 an antiviral response. We report here that Asibi replication triggers the formation of stress granules in
383 human hepatoma cells and epithelial monkey cells. This is consistent with previous studies showing that
384 infection with the vaccine strain 17D induces the formation of stress granules in human dendritic cells
385 and hamster kidney cells [53]. Thus, formation of stress granules seems to be a general feature of

386 flavivirus infection [35,36,54,55]. However, unlike WNV, DENV, ZIKV and the related tick-borne
387 encephalitis virus [35,36,38,54–57], YFV does not seem to efficiently antagonize stress granule
388 biogenesis. YFV may not express proteins that inhibit granule formation. Alternatively, stress granules
389 may not have an antiviral function against YFV and thus the virus has no pressure to evolve an evasion
390 strategy.

391 Stress granules were not detected in Huh7 cells depleted of PKR upon 24 hours of Asibi infection,
392 strongly suggesting a PKR-dependent granule establishment early in infection. Of note, RIG-I signaling
393 was not involved in stress granule assembly, indicating that, whilst the two sensors are both critically
394 implicated in the pro-inflammatory cytokine production, only PKR is able to activate stress granule
395 formation. At 34 hours, very few cells silenced for PKR exhibited stress granules. Small quantities of
396 remaining PKR, below the detection limit of Western blot and qPCR analysis, may be responsible for
397 the formation of these foci. Alternatively, they may form subsequent to the phosphorylation of eIF2α
398 by one of the other three eIF2α kinases. YFV replication and assembly, which takes place within ER
399 membranes [3], likely causes an ER stress and might thus trigger the activation of the ER resident kinase
400 PERK. Since GCN2 is phosphorylated in mouse and human dendritic cells upon infection with 17D
401 [53], this kinase could also potentially contribute to granule formation in Asibi infected cells. This would
402 explain the effect of the GCN2 inhibitor on stress granule formation in our experimental setting.

403 Similar to what was reported in the context of infection with numerous viruses [27,28,58], we
404 showed that RIG-I accumulates in stress granules upon Asibi infection. PKR, MDA5, LGP2 and the
405 DNA sensor cGAS were also shown to concentrate in stress granules in cells infected with a large panel
406 of RNA and DNA viruses [20,22–26]. However, we were unable to detect neither Asibi RNA nor
407 dsRNA structures in stress granules of infected cells. Thus, the interaction between YFV RNA by RIG-
408 I and PKR is unlikely to occur in stress granules. Similarly, in cells infected with Orthohantaviruses, no
409 viral RNA was found associated with stress granules [59]. Conversely, viral RNA was detected in stress
410 granules induced by infection with IAVΔNS1 [20]. We propose that, at least in Asibi-infected cells, the
411 large accumulation of PKR and RIG-I in stress granules masks the detection of small quantities of PKR
412 and RIG-I which are recruited to perinuclear ER-derived replication sites, where viral RNA sensing
413 occurs. Importantly, inhibition of stress granule formation didn't affect the pro-inflammatory cytokine

414 expression by infected hepatocytes, indicating that the anti-viral response and stress granules formation
415 are independent events in the early phases of YFV infection. Whether the formation of stress granules
416 and their composition affect later stages of infection remains to be established.
417 Collectively, our data strongly suggest that, in cells infected with YFV, pro-inflammatory cytokine
418 induction is mediated by RIG-I and PKR, independent of their localization in stress granules. Thus,
419 contrary to the widely believed consensus, we demonstrated that the stress granule formation can be
420 uncoupled from the initiation of a pro-inflammatory response upon viral infection.
421
422
423
424 **Materials and Methods**
425 **Cell lines, virus, antibodies and inhibitors**
426 Huh7 human hepatocellular carcinoma cells (kindly provided by A. Martin, Institut Pasteur Paris)
427 and Huh7.5 cells [60] were maintained in Dulbecco's modified eagle's medium (DMEM)(Gibco)
428 containing GlutaMAX I and sodium pyruvate (Invitrogen) supplemented with 10% heat-inactivated
429 foetal bovine serum (FBS, Dominique Dutscher) and 1% penicillin and streptomycin (P/S, 10.000 U/ml,
430 Thermofischer). HepG2 cells (kindly provided by C. Neuveut, Institut Pasteur Paris) were maintained
431 in DMEM-F12 complemented with 10% FBS, 3.5×10^{-7} M hydrocortisone, and 5 µg/ml insulin. Human
432 embryonic kidney (HEK) 293FT cells (American Type Culture Collection; ATCC CRL-1573), *Macaca*
433 *mulatta* mammary gland epithelial CMMT cells (kindly provided by O. Schwartz, Institut Pasteur Paris)
434 and African green monkey kidney epithelial Vero cells (ATCC) were maintained in DMEM 10% FBS.
435 The Asibi strain, which is the YFV reference strain was provided by the Biological Resource Center
436 of Institut Pasteur. The YFV-DAK strain (YFV-Dakar HD1279) was provided by the World Reference
437 Center for Emerging Viruses and Arboviruses (WRCEVA), through the University of Texas Medical
438 Branch at Galveston, USA. Virus stocks were propagated on Vero cells. Viruses were concentrated by
439 polyethylene glycol 6000 precipitation and purified by centrifugation in a discontinued gradient of
440 sucrose. Infectious virus titers were determined by plaque assays on Vero cells. Cells were infected
441 with 10-fold serial dilutions of viral stocks and incubated for 4 days in DMEM containing 2% FBS and

442 carboxymethyl cellulose. Cells were then washed with PBS, fixed with 3% formaldehyde crystal violet
443 solution for 20 min at room temperature, rinsed with water and plaques were counted. Cell infections
444 were carried out at the indicated MOIs. The viral inoculum was replaced with fresh culture medium two
445 hours post-infection.

446 The following antibodies were used: pIRF3 S386 (clone EPR2346, Abcam), IRF3 (FL-425, Santa
447 Cruz), NF-κB p65 (D14E12, Cell Signalling), IκBα (L35A5, Cell Signalling), β-Actin (clone AC-74,
448 Sigma-Aldrich), dsRNA J2 (English & Scientific Consulting Kft), G3BP (BD Biosciences), TIAR (C-
449 18, Santa-Cruz), eIF4G (sc-11373, Santa-Cruz), eIF3b (N-20, sc-16377), YFV-NS4b (kind gift from
450 C.M. Rice, Rockefeller University), Alexa Fluor® 488 donkey Anti-Goat IgG (H+L), Alexa Fluor®
451 594 donkey Anti-Mouse IgG (H+L), Alexa Fluor® 647 donkey Anti-Rabbit IgG (H+L) (Life
452 Technologies), anti-mouse 680 (LI-COR Bioscience), anti-rabbit 800 (Thermo Fisher Scientific). The
453 RIG-I antibody was previously described [20].

454 BAY11-7085 (Abcam), GSK2606414 (Selleck Chemicals), GCN2-IN-1 (A-92) (Selleck
455 Chemicals) were resuspended in DMSO (Pan Bioteck) and used at the indicated concentration. Sodium
456 arsenite (NaArs, Sigma) and Cycloheximide (CHX, Sigma) were diluted in water.

457

458 **Generation of shRNA-expressing Huh7 cells by lentiviral transduction**

459 pALPS-shPKR1 and pALPS-shPKR3 were generated by cloning the following sequences in
460 pALPS [61]: (TGC TGT TGA CAG TGA GCG CCA GCA GAT ACA TCA GAG ATA ATA GTG
461 AAG CCA CAG ATG TAT TAT CTC TGA TGT ATC TGC TGA TGC CTA CTG CCT CGG A) and
462 (TGC TGT TGA CAG TGA GCG ACA GAA GAA AAG ACT AAC TGT ATA GTG AAG CCA CAG
463 ATG TAT ACA GTT AGT CTT TTC TTC TGG TGC CTA CTG CCT CGG A). HEK293FT cells were
464 transfected with pCMV-VSV-G codon-optimized, pCMVR8.74 (both plasmids were given by P.
465 Charneau, Institut Pasteur) and lentiviral vectors (pALPS-shPKR1/3 or pALPS-shLuc) at a mass ratio
466 of 1:4:4. Huh7 cells were transduced with supernatant from transfected HEK293FT and selected with
467 10 μg/μL puromycin (Sigma Aldrich) four days later.

468

469 **Small Interfering RNA (siRNA) transfection**

470 Huh7 cells were transfected using Lipofectamine RNAiMax (Life Technologies) at 30 nM final of
471 nontargeting scrambled negative control (siScr) or G3BP1, G3BP2 and TIAR siRNAs. Alternatively,
472 cells were transfected at 40 nM final of siRNA-TIA1. All siRNAs were obtained from Dharmacon (ON-
473 TARGETplus SMARTpool). Transfected cells were harvested or used for infection assays 48 hours
474 after transfection.
475
476 **Enzyme-linked immunosorbent assay (ELISA)**
477 The amount of TNFα and IL6 in cell-culture supernatants was quantified by ELISA using the Human
478 TNFα or IL6 ELISA kit (eBiosciences), according to manufacturer's instructions. The detection limits
479 were 4 pg/ml for TNFα and 2 pg/ml for IL6.
480
481 **Western blot analysis**
482 Cells were lysed in radioimmunoprecipitation assay (RIPA) buffer (Sigma) containing a protease and
483 phosphatase inhibitor mixture (Roche). Cell lysates were normalized for protein content, boiled in
484 NuPAGE LDS sample buffer (Thermo Fisher Scientific) in non-reducing conditions and the proteins
485 were separated by SDS-PAGE (NuPAGE 4-12% Bis-Tris Gel, Life Technologies). Proteins were
486 transferred to nitrocellulose membranes (Bio-Rad) using a Trans-Blot Turbo Transfer system (Bio-Rad).
487 After blocking with PBS-Tween-20 0,1% (PBST) containing 5% milk or BSA for 1 hour at RT, the
488 membrane was incubated overnight at 4 °C with primary antibodies diluted in a blocking buffer. Finally,
489 the membrane was incubated for 45 min at RT with secondary antibodies (Anti-rabbit/mouse IgG (H+L)
490 DyLight 680/800) diluted in a blocking buffer, washed, and scanned using an Odyssey CLx infrared
491 imaging system (LI-COR Bioscience).
492
493 **RNA extraction and RT-qPCR analysis**
494 Total RNAs were extracted from cell-lysates using the NucleoSpin RNA II Kit (Macherey-Nagel)
495 following the manufacturer's protocol and were eluted in nuclease-free water. First-strand
496 complementary DNA synthesis was performed with the RevertAid H Minus M-MuLV Reverse
497 Transcriptase (Thermo Fisher Scientific). Quantitative real-time PCR was performed on a real-time PCR

498 system (QuantStudio 6 Flex, Applied Biosystems) with SYBR Green PCR Master Mix (Life
499 Technologies). Data were analyzed with the ΔΔCT method, with all samples normalized to GAPDH.
500 All experiments were performed in technical triplicate. Primers used in this study are: GAPDH (GGT
501 CGG AG TCA ACG GAT TTG and ACT CCA CGA CGT ACT CAG CG), YF-NS3 (GCG TAA GGC
502 TGG AAA GAG TG and CTT CCT CCC TTC ATC CAC AA), TNFA (GCC CAT GTT GTA GCA
503 AAC CC and GGA GGT TGA CCT TGG TCT GG), IL6 (TGC AAT AAC CAC CCC TGA CC and
504 GTG CCC ATG CTA CAT TTG CC), IFNB (AAG CAA TTG TCC AGT CCC A and TGC ATT ACC
505 TGA AGG CCA AG), PKR (CAG AAT TGA CGG AAA GAC TTA CG and CTC TCA AGA GAA
506 TCA TCA CTG GT), G3BP1 (CAG TTA TAT AGA CCG GCG GC and TAT GTC CAA ACC TAC
507 GCG GC), G3BP2 (CAA TCT CAG CCA CCT CGT GT and CCA CAA CGT TTC CAA AAC TCA
508 T), TIAR (CGT CTG GGT TAA CAG ATC AGC and CAT GGG CTG CAC TTT CAT GG), TIA1
509 (AAT CCC GTG CAA CAG CAG GA and AGG CGG TTG CAC TCC ATA AT). Viral genome
510 equivalents concentrations (GE/ml) were determined by extrapolation from a standard curve generated
511 from serial dilutions of the plasmid encoding the YF-R.luc2A-RP [62].
512
513 **Immunofluorescence, fluorescence *in situ* hybridization (FISH) and confocal analysis.**
514 Cells were fixed with 4% paraformaldehyde (PFA; Sigma-Aldrich) for 30 min at RT, permeabilized
515 with 0.5% Triton X-100 in PBS and then blocked with 0,05% Tween-, 5% BSA-containing PBS before
516 incubation with the indicated primary antibodies. Antibody labelling was revealed with Alexa Fluor®
517 488-, 594 or 647-conjugated antibodies. Coverslips were mounted on slides using ProLong® Gold
518 Antifade Reagent with NucBlue solution (Invitrogen). Images were acquired with a Zeiss LSM 700
519 inverted confocal microscope. Fluorescence in situ hybridization was performed after immunostaining.
520 The (+) RNA strands of YFV were detected following the manufacturer's protocol (ViewRNA ISH
521 Cells Assays) using probe sets designed by Affymetrix. The Alexa-Fluor 546-conjugated (+)-strand
522 probe set targets a region between position nucleotides 4567 and 5539 of the YFV genome. Intensity
523 plot data were generated using Zen 2 lite (Zeiss) and plotted using GraphPad Prism 6.
524
525 **Stress granule quantification**

526 Nucleus and stress granule quantifications were performed using CellProfiler (v3.0.0) using custom
527 pipeline (available on request). In a nutshell: (i) nuclei were detected using the NucBlue signal, (ii)
528 cellular border were estimated using TIAR or eiF3b signal, (iii) stress granule borders were estimated
529 using G3BP, TIAR, eIF4G or eIF3b signals. Further analyses were performed using R and R studio [63].
530 Cells were considered positive for stress granules if they exhibited at least two of them.
531
532 **Statistical analysis**
533 Data are presented as means ± SD and were analyzed using GraphPad Prism 6. Statistical analysis of
534 percentage values or fold enrichment values were performed on logit or log-transformed values,
535 respectively. Statistical analysis was performed with two tailed unpaired t-test with Welch correction
536 for pairwise comparisons or by one- or two-way analysis of variance (ANOVA) with Tukey's or
537 Dunnet's multiple comparisons test when comparing more than two sets of values. Each experiment was
538 performed at least twice, unless otherwise stated. Statistically significant differences are indicated as
539 follows: *: $p < 0.05$, **: $p < 0.01$ and ***: $p < 0.001$; ns, not significant.
540

541 **Acknowledgments**. We thank C.M Rice for generously providing the anti-YFV-NS4b antibodies; R.
542 Kuhn for the YFV replicon construct, M. Flamand for anti-NS1 antibodies (17A12), C. Neuveut for the
543 HepG2 cells, O. Schwartz for the CMMT cells, A. Martin for Huh7 cells, P. Schnupf for eIF3b and
544 eIF4G antibodies, P. Charneau for the plasmids pCMV-VSV-G and pCMVR8.74, A. Cimarelli for the
545 pALPS plasmid, Olivier Disson for immuno-histochemistry advice and Léa Richard for cloning shPKR
546 into pALPS. We are grateful to the members of our laboratory for helpful discussions and technical
547 advice. We thank Audrey Salles and Julien Fernandes (UTechS Photonic Bioimaging platform, Institut
548 Pasteur) for their help in confocal acquisition. We are grateful to Stéphane Rigaud (Image Analysis Hub,
549 Institut Pasteur) for his advice in analyzing confocal images and to Vincent Guillemot (Bioinformatics
550 and Biostatistics HUB, Institut Pasteur) for his help in statistical analysis. Finally, we thank Stephanie
551 Straubel for critical reading of the manuscript.

552

553

554 **References**

555 1. Gould EA, Solomon T. Pathogenic flaviviruses. Lancet. 2008;371: 500–9.
556 doi:10.1016/S0140-6736(08)60238-X
557 2. Gubler DJ, Kuno G, Markoff L. Flaviviruses. 5th Edition. Fields Virology. 5th
558 Edition. 2007. pp. 1153–1252.
559 3. Douam F, Ploss A. Yellow Fever Virus: Knowledge Gaps Impeding the Fight Against
560 an Old Foe. Trends Microbiol. 2018;26: 913–928. doi:10.1016/j.tim.2018.05.012
561 4. Pulendran B. Learning immunology from the yellow fever vaccine: innate immunity to
562 systems vaccinology. Nat Rev Immunol. 2009;9: 741–7. doi:nri2629 [pii] 10.1038/nri2629
563 5. Barrett AD. Yellow Fever in Angola and Beyond--The Problem of Vaccine Supply
564 and Demand. N Engl J Med. 2016;375: 301–3. doi:10.1056/NEJMp1606997
565 6. Barrett ADT. The reemergence of yellow fever. Science. 2018;361: 847–848.
566 doi:10.1126/science.aau8225
567 7. Messaoudi I, Basler CF. Immunological features underlying viral hemorrhagic fevers.
568 Curr Opin Immunol. 2015;36: 38–46. doi:10.1016/j.coi.2015.06.003
569 8. Paessler S, Walker DH. Pathogenesis of the viral hemorrhagic fevers. Annu Rev
570 Pathol. 2013;8: 411–40. doi:10.1146/annurev-pathol-020712-164041
571 9. Chen IY, Ichinohe T. Response of host inflammasomes to viral infection. Trends
572 Microbiol. 2015;23: 55–63. doi:10.1016/j.tim.2014.09.007
573 10. ter Meulen J, Sakho M, Koulemou K, Magassouba N, Bah A, Preiser W, et al.
574 Activation of the cytokine network and unfavorable outcome in patients with yellow fever.
575 The Journal of infectious diseases. 2004;190: 1821–7. doi:10.1086/425016
576 11. Engelmann F, Josset L, Girke T, Park B, Barron A, Dewane J, et al. Pathophysiologic
577 and transcriptomic analyses of viscerotropic yellow fever in a rhesus macaque model. PLoS
578 Negl Trop Dis. 2014;8: e3295. doi:10.1371/journal.pntd.0003295
579 12. Streicher F, Jouvenet N. Stimulation of Innate Immunity by Host and Viral RNAs.
580 Trends in Immunology. 2019;40: 1134–1148. doi:10.1016/j.it.2019.10.009
581 13. Chow KT, Gale M, Loo Y-M. RIG-I and Other RNA Sensors in Antiviral Immunity.
582 Annual Review of Immunology. 2018;36: 667–694. doi:10.1146/annurev-immunol-042617-
583 053309
584 14. Nan Y, Nan G, Zhang YJ. Interferon induction by RNA viruses and antagonism by
585 viral pathogens. Viruses. 2014;6: 4999–5027. doi:10.3390/v6124999
586 15. Chazal M, Beauclair G, Gracias S, Najburg V, Simon-Loriere E, Tangy F, et al. RIG-I
587 Recognizes the 5' Region of Dengue and Zika Virus Genomes. Cell Rep. 2018;24: 320–328.
588 doi:10.1016/j.celrep.2018.06.047
589 16. Sprokholt JK, Kaptein TM, van Hamme JL, Overmars RJ, Gringhuis SI, Geijtenbeek
590 TBH. RIG-I-like Receptor Triggering by Dengue Virus Drives Dendritic Cell Immune
591 Activation and TH1 Differentiation. J Immunol. 2017;198: 4764–4771.
592 doi:10.4049/jimmunol.1602121
593 17. Sprokholt JK, Kaptein TM, van Hamme JL, Overmars RJ, Gringhuis SI, Geijtenbeek
594 TBH. RIG-I-like receptor activation by dengue virus drives follicular T helper cell formation
595 and antibody production. PLoS Pathog. 2017;13: e1006738.
596 doi:10.1371/journal.ppat.1006738
597 18. Hertzog J, Junior AGD, Rigby RE, Donald CL, Mayer A, Sezgin E, et al. Infection
598 with a Brazilian isolate of Zika virus generates RIG-I stimulatory RNA and the viral NS5
599 protein blocks type I IFN induction and signaling. European Journal of Immunology.
600 2018;48: 1120–1136. doi:10.1002/eji.201847483
601 19. Bruni D, Chazal M, Sinigaglia L, Chauveau L, Schwartz O, Despres P, et al. Viral

602 entry route determines how human plasmacytoid dendritic cells produce type I interferons.
603 Sci Signal. 2015;8: ra25. doi:10.1126/scisignal.aaa1552
604 20. Onomoto K, Jogi M, Yoo J-S, Narita R, Morimoto S, Takemura A, et al. Critical Role
605 of an Antiviral Stress Granule Containing RIG-I and PKR in Viral Detection and Innate
606 Immunity. PLOS ONE. 2012;7: e43031. doi:10.1371/journal.pone.0043031
607 21. Oh S-W, Onomoto K, Wakimoto M, Onoguchi K, Ishidate F, Fujiwara T, et al.
608 Leader-Containing Uncapped Viral Transcript Activates RIG-I in Antiviral Stress Granules.
609 PLOS Pathogens. 2016;12: e1005444. doi:10.1371/journal.ppat.1005444
610 22. Yoo J-S, Takahasi K, Ng CS, Ouda R, Onomoto K, Yoneyama M, et al. DHX36
611 enhances RIG-I signaling by facilitating PKR-mediated antiviral stress granule formation.
612 PLoS Pathog. 2014;10: e1004012. doi:10.1371/journal.ppat.1004012
613 23. Sánchez-Aparicio MT, Ayllón J, Leo-Macias A, Wolff T, García-Sastre A. Subcellular
614 Localizations of RIG-I, TRIM25, and MAVS Complexes. J Virol. 2017;91.
615 doi:10.1128/JVI.01155-16
616 24. Langereis MA, Feng Q, Kuppeveld FJ van. MDA5 Localizes to Stress Granules, but
617 This Localization Is Not Required for the Induction of Type I Interferon. Journal of Virology.
618 2013;87: 6314–6325. doi:10.1128/JVI.03213-12
619 25. Narita R, Takahasi K, Murakami E, Hirano E, Yamamoto SP, Yoneyama M, et al. A
620 Novel Function of Human Pumilio Proteins in Cytoplasmic Sensing of Viral Infection. PLOS
621 Pathogens. 2014;10: e1004417. doi:10.1371/journal.ppat.1004417
622 26. Hu S, Sun H, Yin L, Li J, Mei S, Xu F, et al. PKR-dependent cytosolic cGAS foci are
623 necessary for intracellular DNA sensing. Sci Signal. 2019;12. doi:10.1126/scisignal.aav7934
624 27. Onomoto K, Yoneyama M, Fung G, Kato H, Fujita T. Antiviral innate immunity and
625 stress granule responses. Trends Immunol. 2014;35: 420–428. doi:10.1016/j.it.2014.07.006
626 28. McCormick C, Khaperskyy DA. Translation inhibition and stress granules in the
627 antiviral immune response. Nat Rev Immunol. 2017;17: 647–660. doi:10.1038/nri.2017.63
628 29. Ivanov P, Kedersha N, Anderson P. Stress Granules and Processing Bodies in
629 Translational Control. Cold Spring Harb Perspect Biol. 2019;11: a032813.
630 doi:10.1101/cshperspect.a032813
631 30. Reineke LC, Lloyd RE. Diversion of stress granules and P-bodies during viral
632 infection. Virology. 2013;436: 255–267. doi:10.1016/j.virol.2012.11.017
633 31. Sumpter R, Loo YM, Foy E, Li K, Yoneyama M, Fujita T, et al. Regulating
634 intracellular antiviral defense and permissiveness to hepatitis C virus RNA replication
635 through a cellular RNA helicase, RIG-I. J Virol. 2005;79: 2689–99.
636 doi:10.1128/JVI.79.5.2689-2699.2005
637 32. Pierce JW, Schoenleber R, Jesmok G, Best J, Moore SA, Collins T, et al. Novel
638 inhibitors of cytokine-induced IkappaBalpha phosphorylation and endothelial cell adhesion
639 molecule expression show anti-inflammatory effects in vivo. J Biol Chem. 1997;272: 21096–
640 103.
641 33. Ivanov P, Kedersha N, Anderson P. Stress Granules and Processing Bodies in
642 Translational Control. [cited 17 Jan 2020]. doi:10.1101/cshperspect.a032813
643 34. Kedersha N, Cho MR, Li W, Yacono PW, Chen S, Gilks N, et al. Dynamic Shuttling
644 of Tia-1 Accompanies the Recruitment of mRNA to Mammalian Stress Granules. J Cell Biol.
645 2000;151: 1257–1268. doi:10.1083/jcb.151.6.1257
646 35. Bonenfant G, Williams N, Netzband R, Schwarz MC, Evans MJ, Pager CT. Zika
647 Virus Subverts Stress Granules To Promote and Restrict Viral Gene Expression. Journal of
648 Virology. 2019;93. doi:10.1128/JVI.00520-19
649 36. Emara MM, Brinton MA. Interaction of TIA-1/TIAR with West Nile and dengue virus
650 products in infected cells interferes with stress granule formation and processing body
651 assembly. Proceedings of the National Academy of Sciences. 2007;104: 9041–9046.

652 doi:10.1073/pnas.0703348104
653 37. Monath TP. Yellow fever vaccine. Expert review of vaccines. 2005;4: 553–74.
654 doi:10.1586/14760584.4.4.553
655 38. Hou S, Kumar A, Xu Z, Airo AM, Stryapunina I, Wong CP, et al. Zika Virus Hijacks
656 Stress Granule Proteins and Modulates the Host Stress Response. Journal of Virology.
657 2017;91. doi:10.1128/JVI.00474-17
658 39. Tu Y-C, Yu C-Y, Liang J-J, Lin E, Liao C-L, Lin Y-L. Blocking Double-Stranded
659 RNA-Activated Protein Kinase PKR by Japanese Encephalitis Virus Nonstructural Protein
660 2A. Journal of Virology. 2012;86: 10347–10358. doi:10.1128/JVI.00525-12
661 40. Samuel MA, Whitby K, Keller BC, Marri A, Barchet W, Williams BRG, et al. PKR
662 and RNase L Contribute to Protection against Lethal West Nile Virus Infection by Controlling
663 Early Viral Spread in the Periphery and Replication in Neurons. J Virol. 2006;80: 7009–7019.
664 doi:10.1128/JVI.00489-06
665 41. Dabo S, Meurs EF. dsRNA-Dependent Protein Kinase PKR and its Role in Stress,
666 Signaling and HCV Infection. Viruses. 2012;4: 2598–2635. doi:10.3390/v4112598
667 42. Lu L, Han AP, Chen JJ. Translation initiation control by heme-regulated eukaryotic
668 initiation factor 2alpha kinase in erythroid cells under cytoplasmic stresses. Mol Cell Biol.
669 2001;21: 7971–7980. doi:10.1128/MCB.21.23.7971-7980.2001
670 43. Axten JM, Medina JR, Feng Y, Shu A, Romeril SP, Grant SW, et al. Discovery of 7-
671 methyl-5-(1-{[3-(trifluoromethyl)phenyl]acetyl}-2,3-dihydro-1H-indol-5-yl)-7H-pyrrolo[2,3-
672 d]pyrimidin-4-amine (GSK2606414), a potent and selective first-in-class inhibitor of protein
673 kinase R (PKR)-like endoplasmic reticulum kinase (PERK). J Med Chem. 2012;55: 7193–
674 7207. doi:10.1021/jm300713s
675 44. Bonnet MC, Weil R, Dam E, Hovanessian AG, Meurs EF. PKR stimulates NF-kappaB
676 irrespective of its kinase function by interacting with the IkappaB kinase complex. Mol Cell
677 Biol. 2000;20: 4532–4542. doi:10.1128/mcb.20.13.4532-4542.2000
678 45. Bonnet MC, Daurat C, Ottone C, Meurs EF. The N-terminus of PKR is responsible for
679 the activation of the NF-κB signaling pathway by interacting with the IKK complex. Cellular
680 Signalling. 2006;18: 1865–1875. doi:10.1016/j.cellsig.2006.02.010
681 46. Sinigaglia L, Gracias S, Decembre E, Fritz M, Bruni D, Smith N, et al. Immature
682 particles and capsid-free viral RNA produced by Yellow fever virus-infected cells stimulate
683 plasmacytoid dendritic cells to secrete interferons. Sci Rep. 2018;8: 10889.
684 doi:10.1038/s41598-018-29235-7
685 47. Errett JS, Suthar MS, McMillan A, Diamond MS, Gale M. The essential,
686 nonredundant roles of RIG-I and MDA5 in detecting and controlling West Nile virus
687 infection. J Virol. 2013;87: 11416–25. doi:10.1128/JVI.01488-13
688 48. Zamanian-Daryoush M, Mogensen TH, DiDonato JA, Williams BR. NF-kappaB
689 activation by double-stranded-RNA-activated protein kinase (PKR) is mediated through NF-
690 kappaB-inducing kinase and IkappaB kinase. Mol Cell Biol. 2000;20: 1278–1290.
691 doi:10.1128/mcb.20.4.1278-1290.2000
692 49. Pham AM, Santa Maria FG, Lahiri T, Friedman E, Marié IJ, Levy DE. PKR
693 Transduces MDA5-Dependent Signals for Type I IFN Induction. PLoS Pathog. 2016;12.
694 doi:10.1371/journal.ppat.1005489
695 50. Gil J, García MA, Gomez-Puertas P, Guerra S, Rullas J, Nakano H, et al. TRAF
696 Family Proteins Link PKR with NF-κB Activation. Molecular and Cellular Biology. 2004;24:
697 4502–4512. doi:10.1128/MCB.24.10.4502-4512.2004
698 51. Arnaud N, Dabo S, Akazawa D, Fukasawa M, Shinkai-Ouchi F, Hugon J, et al.
699 Hepatitis C virus reveals a novel early control in acute immune response. PLoS Pathog.
700 2011;7: e1002289. doi:10.1371/journal.ppat.1002289 PPATHOGENS-D-11-00682 [pii]
701 52. Zhang P, Li Y, Xia J, He J, Pu J, Xie J, et al. IPS-1 plays an essential role in dsRNA-

702 induced stress granule formation by interacting with PKR and promoting its activation. J Cell
703 Sci. 2014;127: 2471–2482. doi:10.1242/jcs.139626
704 53. Ravindran R, Khan N, Nakaya HI, Li S, Loebbermann J, Maddur MS, et al. Vaccine
705 activation of the nutrient sensor GCN2 in dendritic cells enhances antigen presentation.
706 Science. 2014;343: 313–317. doi:10.1126/science.1246829
707 54. Albornoz A, Carletti T, Corazza G, Marcello A. The stress granule component TIA-1
708 binds tick-borne encephalitis virus RNA and is recruited to perinuclear sites of viral
709 replication to inhibit viral translation. J Virol. 2014;88: 6611–6622. doi:10.1128/JVI.03736-
710 13
711 55. Roth H, Magg V, Uch F, Mutz P, Klein P, Haneke K, et al. Flavivirus Infection
712 Uncouples Translation Suppression from Cellular Stress Responses. mBio. 2017;8.
713 doi:10.1128/mBio.02150-16
714 56. Basu M, Courtney SC, Brinton MA. Arsenite-induced stress granule formation is
715 inhibited by elevated levels of reduced glutathione in West Nile virus-infected cells. PLOS
716 Pathogens. 2017;13: e1006240. doi:10.1371/journal.ppat.1006240
717 57. Amorim R, Temzi A, Griffin BD, Mouland AJ. Zika virus inhibits eIF2α-dependent
718 stress granule assembly. PLOS Neglected Tropical Diseases. 2017;11: e0005775.
719 doi:10.1371/journal.pntd.0005775
720 58. Zhang Q, Sharma NR, Zheng Z-M, Chen M. Viral Regulation of RNA Granules in
721 Infected Cells. Virol Sin. 2019;34: 175–191. doi:10.1007/s12250-019-00122-3
722 59. Christ W, Tynell J, Klingström J. Puumala and Andes Orthohantaviruses Cause
723 Transient Protein Kinase R-Dependent Formation of Stress Granules. J Virol. 2020;94.
724 doi:10.1128/JVI.01168-19
725 60. Blight KJ, McKeating JA, Rice CM. Highly permissive cell lines for subgenomic and
726 genomic hepatitis C virus RNA replication. J Virol. 2002;76: 13001–14.
727 61. Pertel T, Hausmann S, Morger D, Zuger S, Guerra J, Lascano J, et al. TRIM5 is an
728 innate immune sensor for the retrovirus capsid lattice. Nature. 2011;472: 361–5.
729 doi:10.1038/nature09976
730 62. Jones CT, Patkar CG, Kuhn RJ. Construction and applications of yellow fever virus
731 replicons. Virology. 2005;331: 247–59. doi:10.1016/j.virol.2004.10.034
732 63. RStudio Team. RStudio: Integrated Development Environment for R. 2016.
733

734

735 **Figure legends**

736

737 **Fig 1: The Asibi strain of YFV triggers the production of pro-inflammatory cytokines in hepatoma**
738 **cells through RIG-I, IRF3 and NF-κB**

739 Huh7 and Huh7.5 cells were left uninfected or infected with Asibi at an MOI of 1 for 24 or 48 hours in
740 the absence or presence of 10 µM of BAY11-7085 (BAY). The relative amounts of *IL6* (**A**), *TNFA* (**B**)
741 and *IFNB* (**C**) mRNAs were determined by RT-qPCR analysis and normalized to GAPDH mRNA and
742 non-infected samples. The relative amounts of cell-associated viral RNA were determined by RT-qPCR
743 analysis (**D**) and expressed as genome equivalents (YFV-GE) per µg of total cellular RNA. The data are
744 the means ± SD of two (Huh7.5) or three (Huh7, Huh7+BAY) independent experiments. ns: non-
745 significant, *: $p<0.05$, **: $p<0.01$. (**E**, **F**) Culture media of the indicated cells were analysed by ELISA
746 to determine the amounts of secreted IL6 (**E**) and TNFα (**F**). The data are the means ± SD of two
747 (Huh7.5) or three (Huh7, Huh7+BAY). The dashed lines indicate the limit of detection of the IL6 and
748 TNFα ELISA (2 and 4 pg/ml, respectively). (**G**) Whole-cell lysates of the indicated cells were analysed
749 by Western blotting with antibodies against the indicated proteins. (**H**, **I**) Huh7 cells were left uninfected
750 (NI) or infected with YFV-Asibi for 48 hours at an MOI of 20. Cells were then stained with IRF3 (**H**)
751 or p65 (**I**) (red), dsRNA (green) antibodies and NucBlue® (blue). Around 200 cells per independent
752 experiment were scored for nuclear translocation of IRF3 or p65 (**H** and **I**, respectively). ns: non-
753 significant, *: $p<0.05$.

754

755 **Fig 2: RIG-I localizes to stress granules in Huh7 cells infected with YFV**

756 (**A**) Huh7 cells were left uninfected (NI) or infected with Asibi at MOI of 20 for 24 hours. Cells were
757 then stained with dsRNA (red), RIG-I (purple), TIAR (green) antibodies and NucBlue® (blue). (**B**)
758 Huh7 cells were left uninfected (NI), treated with 0.5 mM NaArs for 30 min or infected with Asibi at
759 an MOI of 20 for the indicated time. Cells were then stained with NS4b (purple), G3BP (red), TIAR
760 (green) antibodies and NucBlue® (blue). Percentage of NS4b-positive and G3BP-positive cells were
761 estimated and shown in purple and yellow respectively. (**C**) Huh7 cells were treated with 0.5 mM NaArs
762 for 30 min or infected with YFV-Asibi at MOI of 20 for 48 hours. Cells were then left untreated (NT)

763 or treated with 100 µg/mL Cycloheximide (CHX) for 1 hour and stained with antibodies against NS4b
764 (purple), TIAR (green) and G3BP (red), as well as with NucBlue® (blue).
765
766 **Fig 3: YFV infection induces the formation of stress granules in several mammalian cells**
767 HepG2 or CMMT cells were infected with Asibi at MOI of 20 for, respectively, 48 and 24 hours. Huh7
768 cells were infected with YFV-HD Dakar at MOI of 10 for 24 hours. Cells were then stained with NS4b
769 (purple), TIAR (green), G3BP (red) antibodies and NucBlue® (blue).
770
771 **Fig 4: PKR contributes to stress granule formation in Asibi-infected Huh7 cells**
772 (**A**) Huh7 cells were left uninfected (NI) or infected with Asibi at an MOI of 20 for 24 or 48 hours.
773 Whole-cell lysates were analysed by Western blotting with antibodies against the indicated proteins.
774 Samples were loaded on the same gel. *: unspecific bands. (**B**) Whole-cell lysates of Huh7-shLuc and
775 Huh7-shPKR cells were analysed by Western blotting with antibodies against the indicated proteins.
776 (**C**) Huh7-shLuc and Huh7-shPKR cells were treated with 0.5 mM NaArs for 30 min and stained with
777 TIAR (green) and G3BP (red) antibodies, as well as with NucBlue® (blue). (**D**) Huh7 cells were left
778 uninfected (NI) or infected with YFV-Asibi at MOI of 2 or 20 for 24 or 34 hours. Cells were then stained
779 with NS4b (purple), TIAR (green), G3BP (red) antibodies and NucBlue® (blue). Images are
780 representative of two independent experiments. Percentage of G3BP-positive (**E**) or NS4b-positive cells
781 (**F**) were estimated by analysing at least 200 cells per condition. ns: non-significant, *: $p<0.05$, **:
782 $p<0.01$, ***: $p<0.001$.
783
784 **Fig 5: PERK and GCN2 contribute to stress granule formation in Asibi-infected cells**
785 Huh7 cells were left uninfected (NI) or infected with Asibi at an MOI of 20 for 24 hours. Cells were
786 then treated for 4 hours with either DMSO, 10 µM GSK2606414 (GSK) or 10 µM GCN2-IN-1 (A-92)
787 (iGCN2) and stained with NS4b (purple), TIAR (green), G3BP (red) antibodies and NucBlue® (blue).
788
789 **Fig 6: PKR contributes to innate response in Asibi-infected Huh7 cells**

790 Huh7-shLuc or -shPKR cells were left uninfected (NI) or infected with Asibi at MOI of 2 or 20 for 24
791 or 34 hours. The relative amounts of (A) *PKR* mRNA, (B) YFV RNA, (C) *IL6* mRNA, (D) *TNFA* mRNA
792 and (E) *IFNB* mRNA were determined by qPCR analysis and normalized to that of GAPDH mRNA and
793 non-infected shLuc samples. Mean ± SD is represented. One-way ANOVA on log transformed data
794 with Tukey corrected multiple comparisons tests were performed. shPKR samples were compared to
795 shLuc ones. ns: non-significant, *: $p<0.05$, **: $p<0.01$, ***: $p<0.001$.
796
797 **Fig 7: Knock-down of G3BP1, G3BP2, TIAR and TIA1 inhibits stress granules formation**
798 (**A**) Huh7 cells were transfected with scramble siRNA (siScr) or with siRNA targeting G3BP1, G3BP2,
799 TIAR and TIA1 (siSG) 48 and 24 hours prior to Asibi infection. Transfected cells were left uninfected
800 (NI), treated with 0.5 mM NaArs for 30 min (NaArs) or infected with Asibi at MOI of 2 or 20 for 24 or
801 34 hours. Cells were then stained with NS1 (purple), eIF3b (green), eIF4G (red) antibodies and
802 NucBlue® (blue). Images are representative of two independent confocal microscopy analyses.
803 Percentages of eIF4G- and eIF3b-positive (**B**) or NS1-positive cells (**C**) were estimated. (**D**) Stress
804 granule area was determined for each cell as the sum of the whole area occupied by stress granules
805 divided by the total cell surface. (**B-D**) Around 200 cells per independent experiment were scored. ns:
806 non-significant, *: $p<0.05$, **: $p<0.01$, ***: $p<0.001$.
807
808 **Fig 8: Inhibition of stress granule formation has limited effect on antiviral response**
809 Huh7 cells were transfected with scramble siRNA (siScr) or with four pools of siRNA targeting G3BP1,
810 G3BP2, TIAR and TIA1 (siSG) 48 and 24 hours prior to infection. Transfected cells were left uninfected
811 (NI) or infected with Asibi at an MOI of 2 or 20. Cells were harvested prior to infection (0 h), 24 or 34
812 hours post-infection. The relative amount of (A) *G3BP1* mRNA, (B) *G3BP2* mRNA, (C) *TIAR* mRNA,
813 (D) *TIA1* mRNA, (E) YFV RNA, (F) *IL6* mRNA, (G) *TNFA* mRNA and (H) *IFNB* mRNA was
814 determined by qPCR analysis and normalized to that of GAPDH mRNA and non-infected sh-Scr
815 samples. Mean ± SD is represented. One-way ANOVA on log transformed data with Tukey corrected
816 multiple comparisons test were performed. Samples treated with siSG-RNA were compared to siScr
817 samples. ns: non-significant, *: $p<0.05$, **: $p<0.01$, ***: $p<0.001$.

818

819 **Fig 9: RIG-I signaling is not involved in stress granule assembly**

820 (**A**) Huh7 and Huh7.5 cells were left uninfected (NI), treated with 0.5 mM NaArs for 30 min (NaArs)
821 or infected with Asibi at MOI of 2 or 20 for 24 or 34 hours. Cells were then stained with NS4b (purple),
822 TIAR (green), G3BP (red) antibodies and NucBlue® (blue). (**B-C**) Images are representative of two
823 independent confocal microscopy analyses. Around 200 cells per independent experiment were scored.
824 Percentages of G3BP-positive (**B**) or NS4b-positive cells (**C**) were estimated. ns: non-significant, *:
825 $p<0.05$, **: $p<0.01$, ***: $p<0.001$.

826

827 **Fig 10: YFN RNA is excluded form stress granules**

828 (**A**) Huh7 cells were left uninfected (NI) or infected with Asibi at MOI of 20 for 24 hours. Cells were
829 then stained with TIAR (green) and NucBlue® (blue), prior to be processed for FISH using a probe
830 specific for YFV (+) strand RNA (red). (**B**) Huh7 cells were left untreated (NT) or treated with 0.5 mM
831 NaArs for 30 min. Cells were then stained with RIG-I (purple), TIAR (green) antibodies and NucBlue®
832 (blue).

833

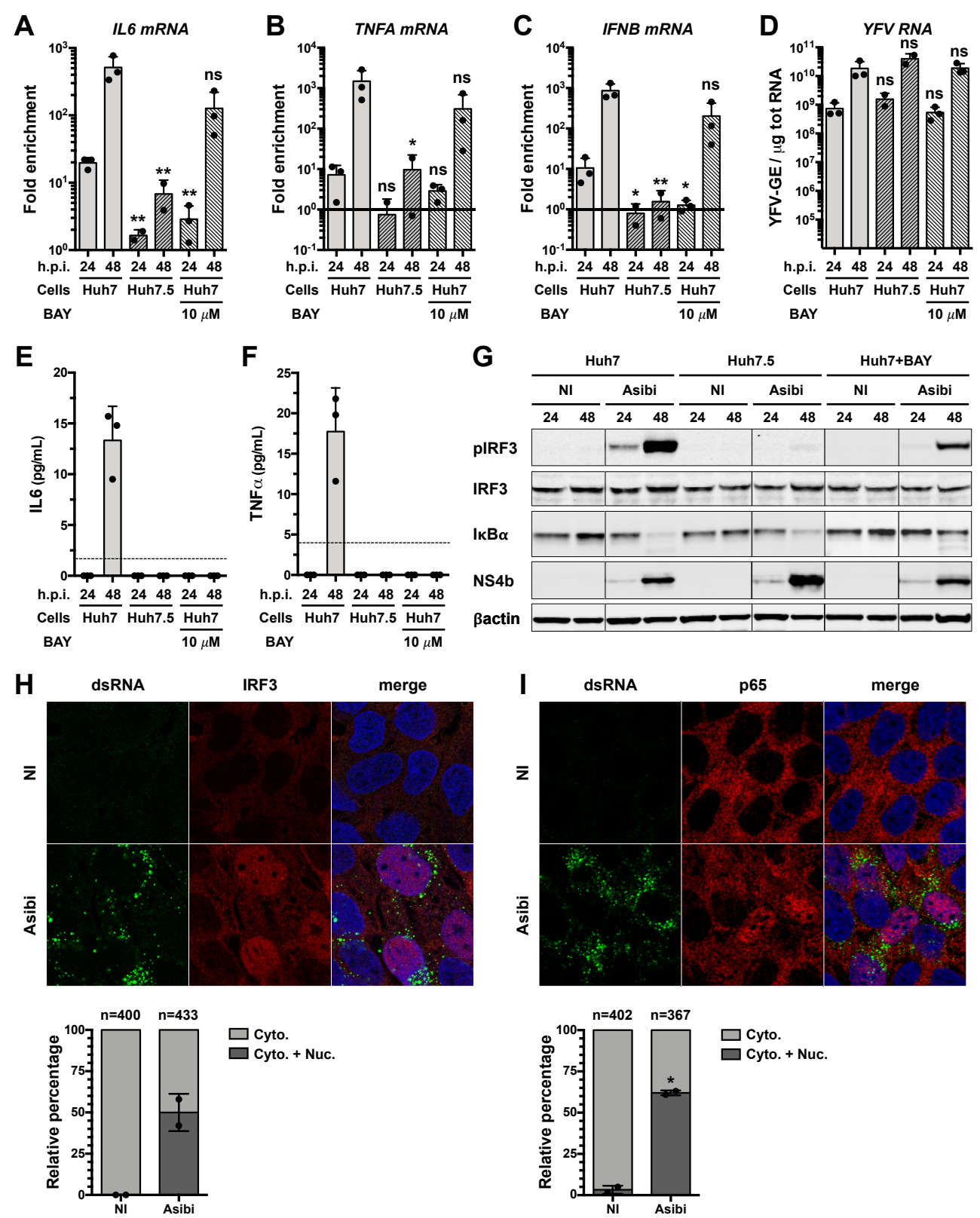
A
IL6 mRNA
Fold enrichment
B
TNFA mRNA
Fold enrichment
C
IFNB mRNA
Fold enrichment
D
YFV RNA
YFV-GE / µg tot RNA
h.p.i. 24 48 24 48 24 48
Cells Huh7 Huh7.5 Huh7
BAY 10 µM
ns
E
IL6 (pg/mL)
F
TNFα (pg/mL)
G
Huh7
Huh7.5
Huh7+BAY
NI
Asibi
pIRF3
IRF3
IκBα
NS4b
βactin
H
dsRNA
IRF3
merge
NI
Asibi
n=400
n=433
Cyto.
Cyto. + Nuc.
Relative percentage
I
dsRNA
p65
merge
n=402
n=367

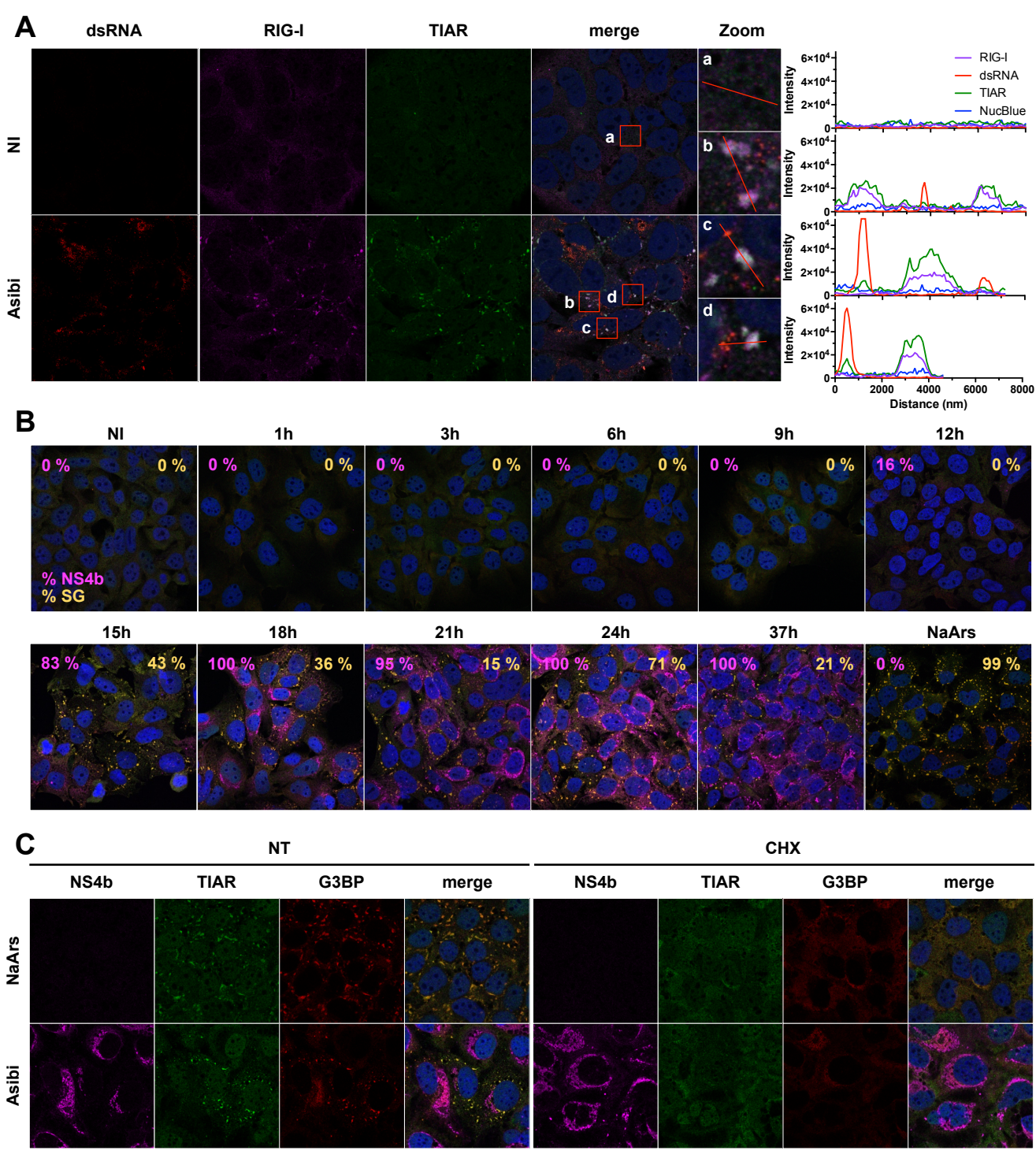
A
dsRNA
RIG-I
TIAR
merge
Zoom
NI
Asibi
a
b
c
d
RIG-I
dsRNA
TIAR
NucBlue
Intensity
Distance (nm)
B
NI
1h
3h
6h
9h
12h
15h
18h
21h
24h
37h
NaArs
% NS4b
% SG
C
NT
CHX
NS4b
TIAR
G3BP
merge
NaArs
Asibi

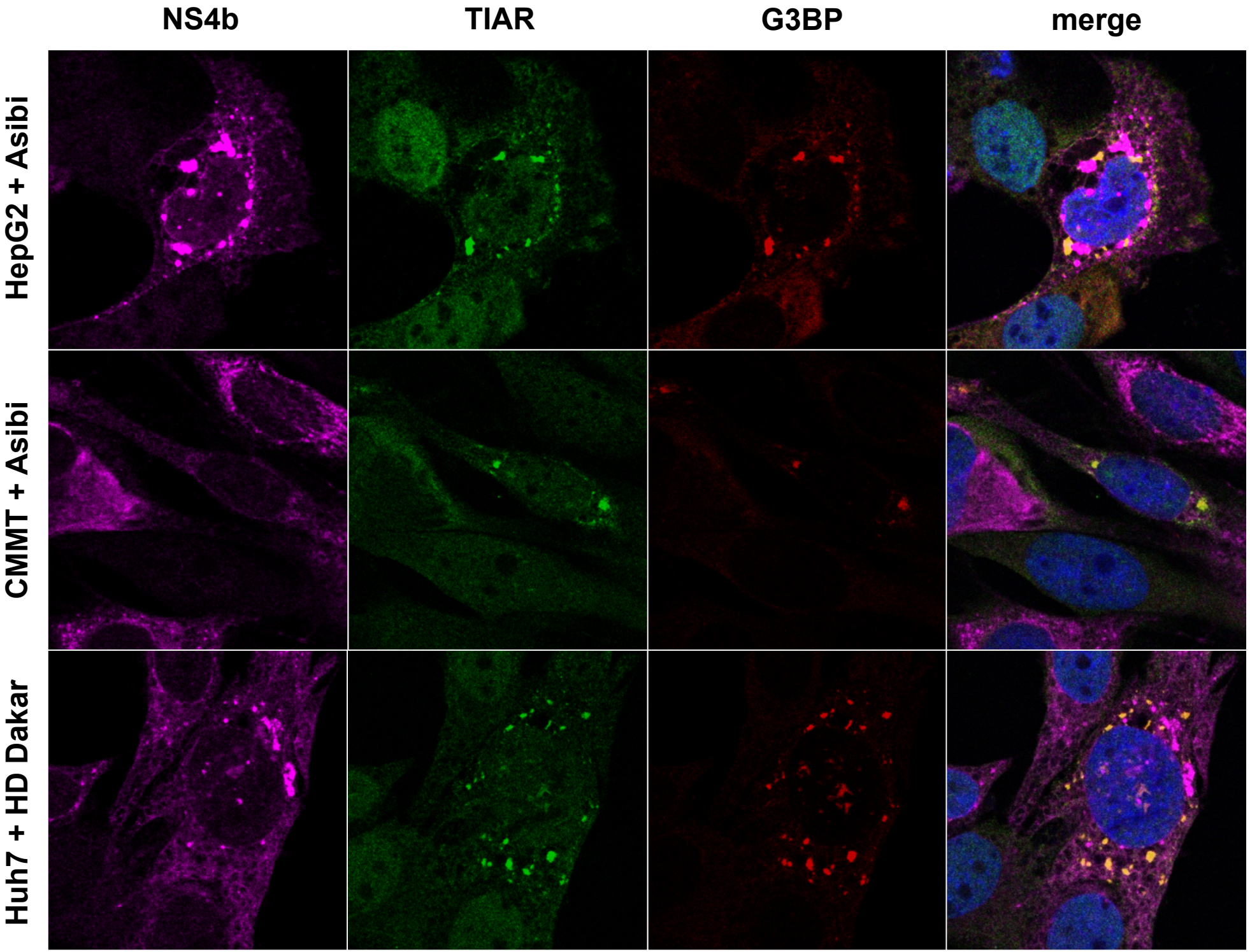
NS4b
TIAR
G3BP
merge
HepG2 + Asibi
CMMT + Asibi
Huh7 + HD Dakar

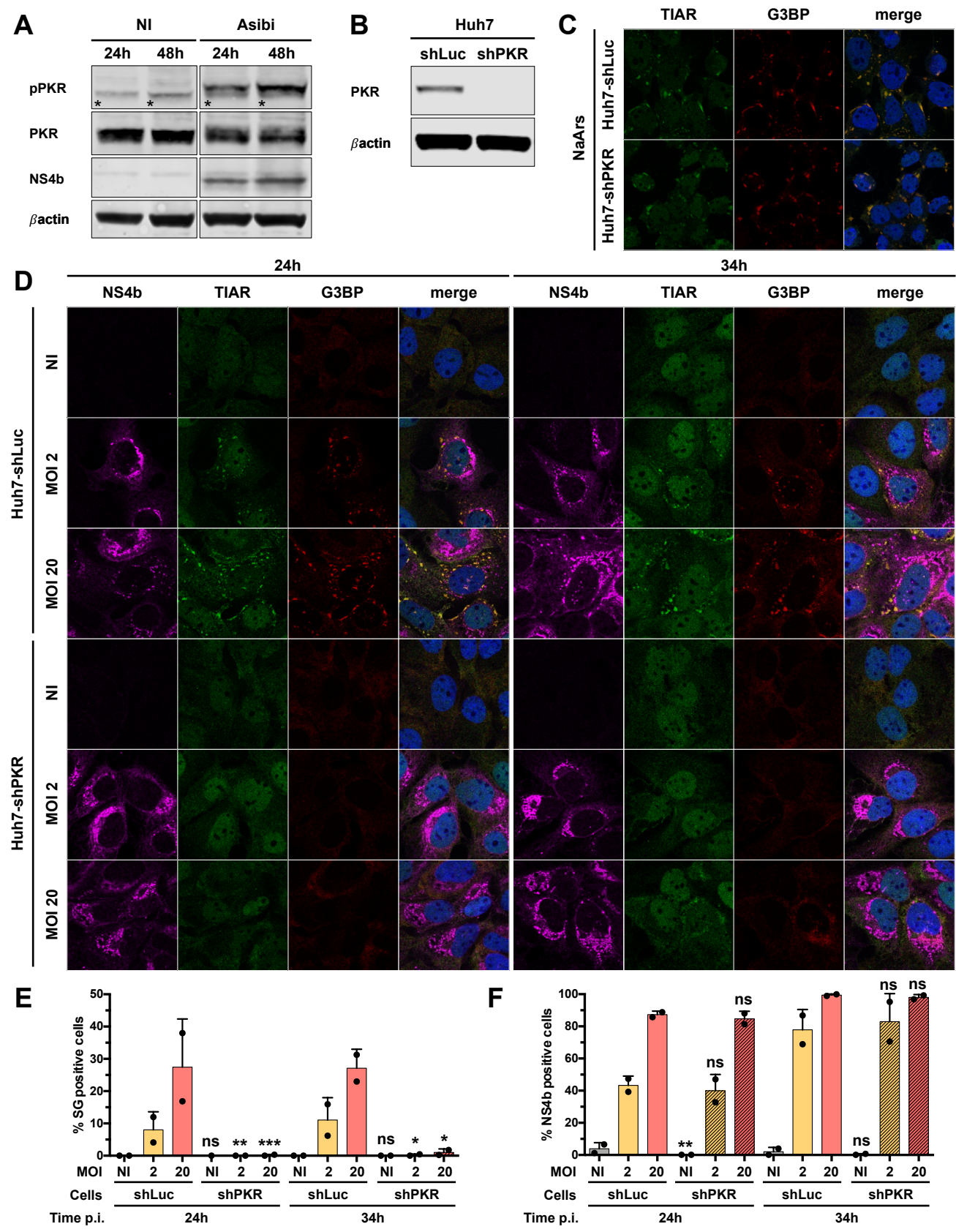
A
NI
Asibi
24h
48h
24h
48h
pPKR
PKR
NS4b
βactin
B
Huh7
shLuc
shPKR
PKR
βactin
C
TIAR
G3BP
merge
NaArs
Huh7-shLuc
Huh7-shPKR
D
24h
34h
NS4b
TIAR
G3BP
merge
Huh7-shLuc
Huh7-shPKR
NI
MOI 2
MOI 20
E
% SG positive cells
MOI
Cells
Time p.i.
shLuc
shPKR
24h
34h
ns
**
***
*
F
% NS4b positive cells
MOI
Cells
Time p.i.
shLuc
shPKR
24h
34h
ns
**

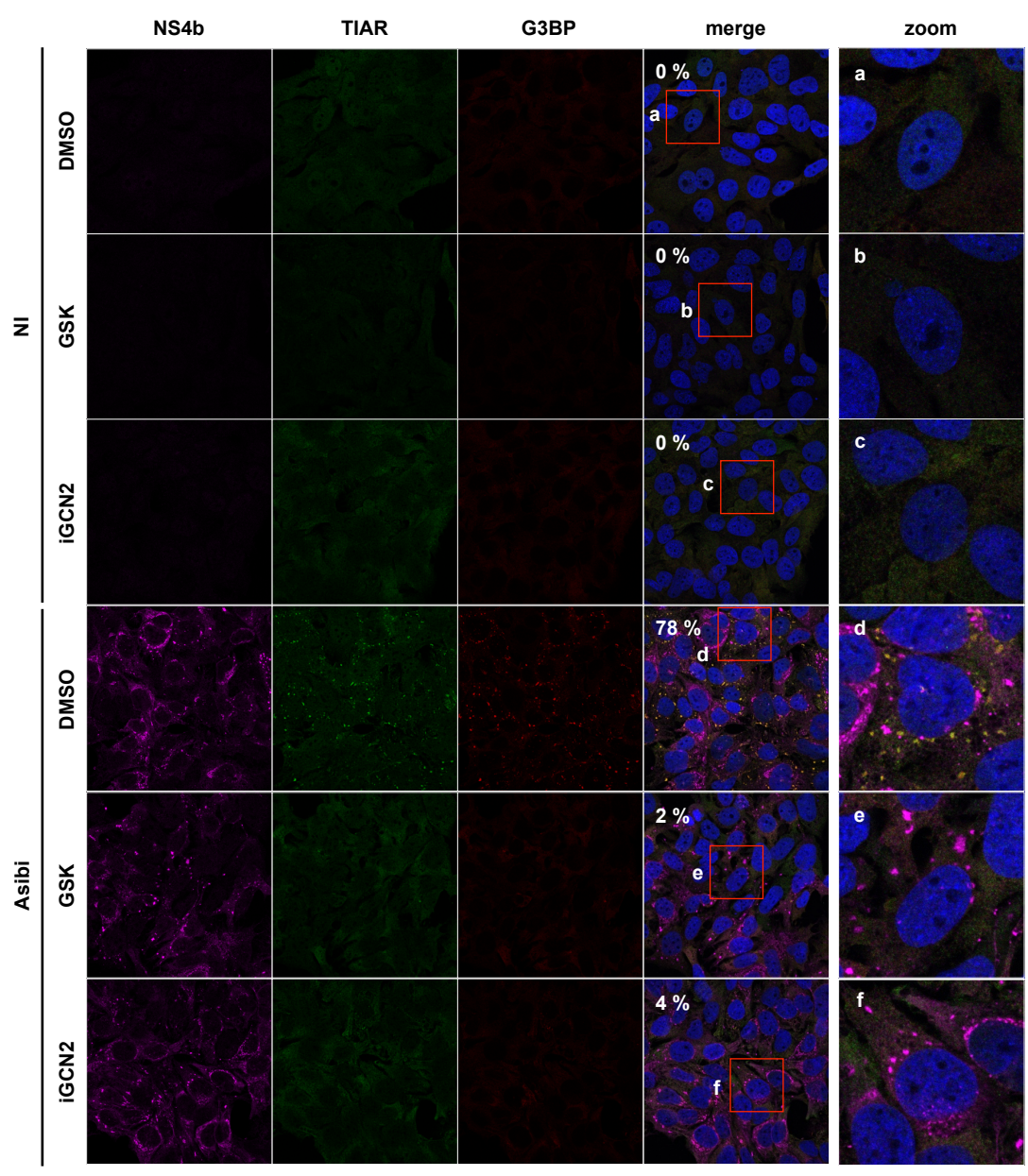
NS4b
TIAR
G3BP
merge
zoom
NI
Asibi
DMSO
GSK
iGCN2
DMSO
GSK
iGCN2
0 %
0 %
0 %
78 %
2 %
4 %
a
b
c
d
e
f

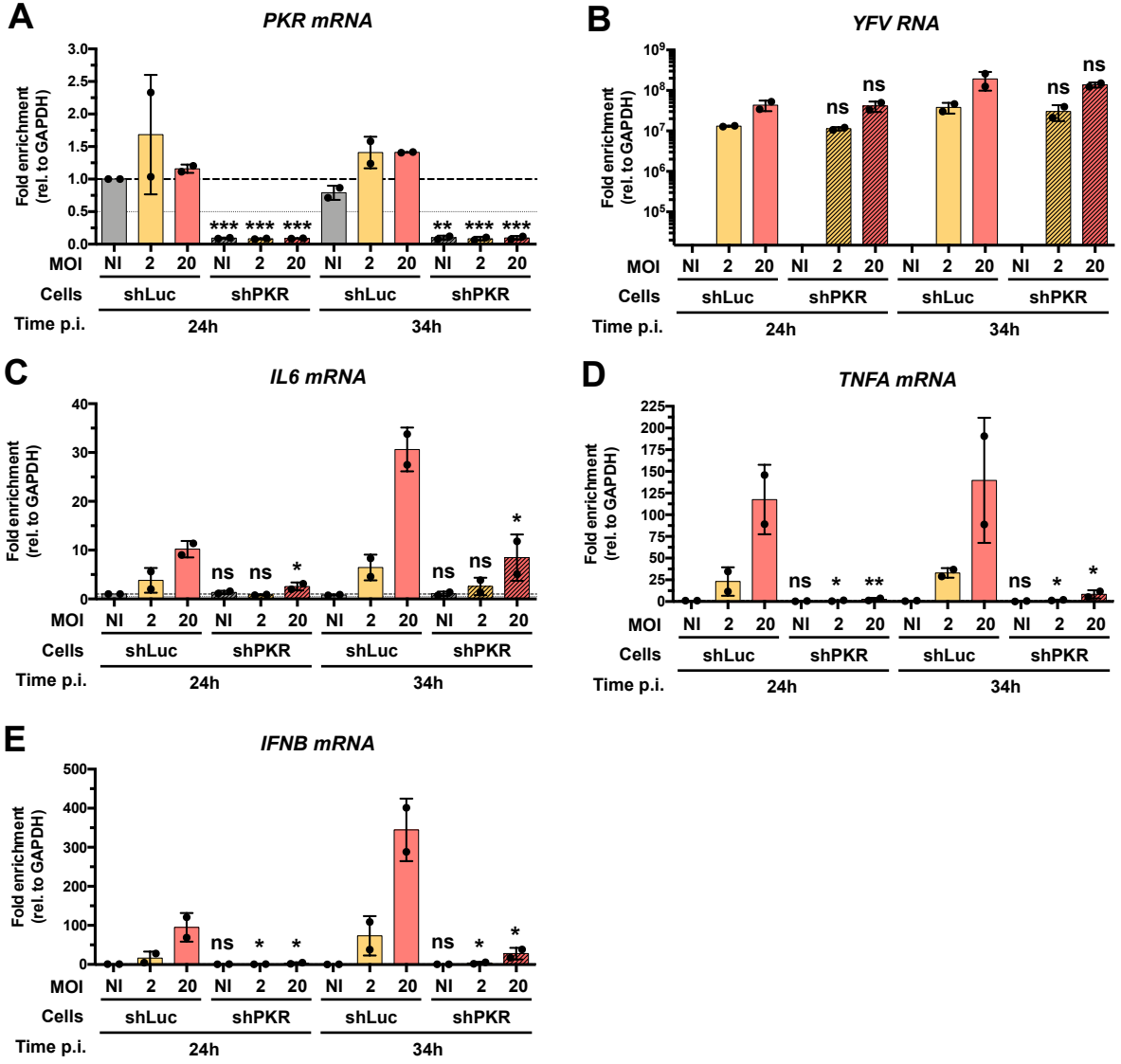
A
PKR mRNA
Fold enrichment (rel. to GAPDH)
3.0
2.5
2.0
1.5
1.0
0.5
0.0
***
***
***
**
***
***
MOI
NI
2
20
Cells
shLuc
shPKR
Time p.i.
24h
34h
B
YFV RNA
Fold enrichment (rel. to GAPDH)
10^9
10^8
10^7
10^6
10^5
ns
ns
ns
ns
C
IL6 mRNA
Fold enrichment (rel. to GAPDH)
40
30
20
10
0
ns
ns
*
ns
ns
*
D
TNFA mRNA
Fold enrichment (rel. to GAPDH)
225
200
175
150
125
100
75
50
25
0
ns
*
**
ns
*
*
E
IFNB mRNA
Fold enrichment (rel. to GAPDH)
500
400
300
200
100
0
ns
*
*
ns
*
*

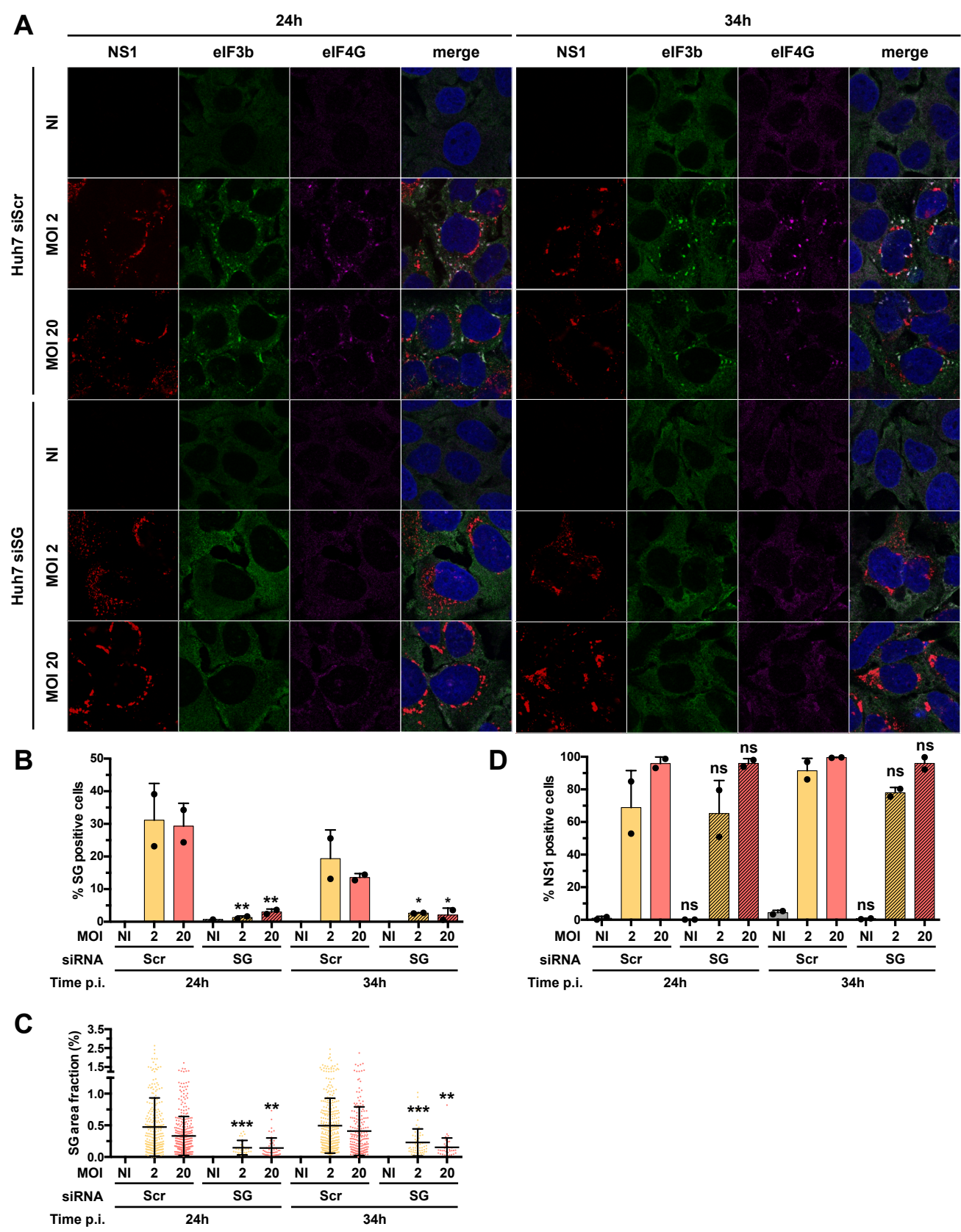
A
24h
34h
NS1
eIF3b
eIF4G
merge
Huh7 siScr
Huh7 siSG
NI
MOI 2
MOI 20
B
% SG positive cells
MOI
siRNA
Scr
SG
Time p.i.
24h
34h
C
SG area fraction (%)
D
% NS1 positive cells
ns

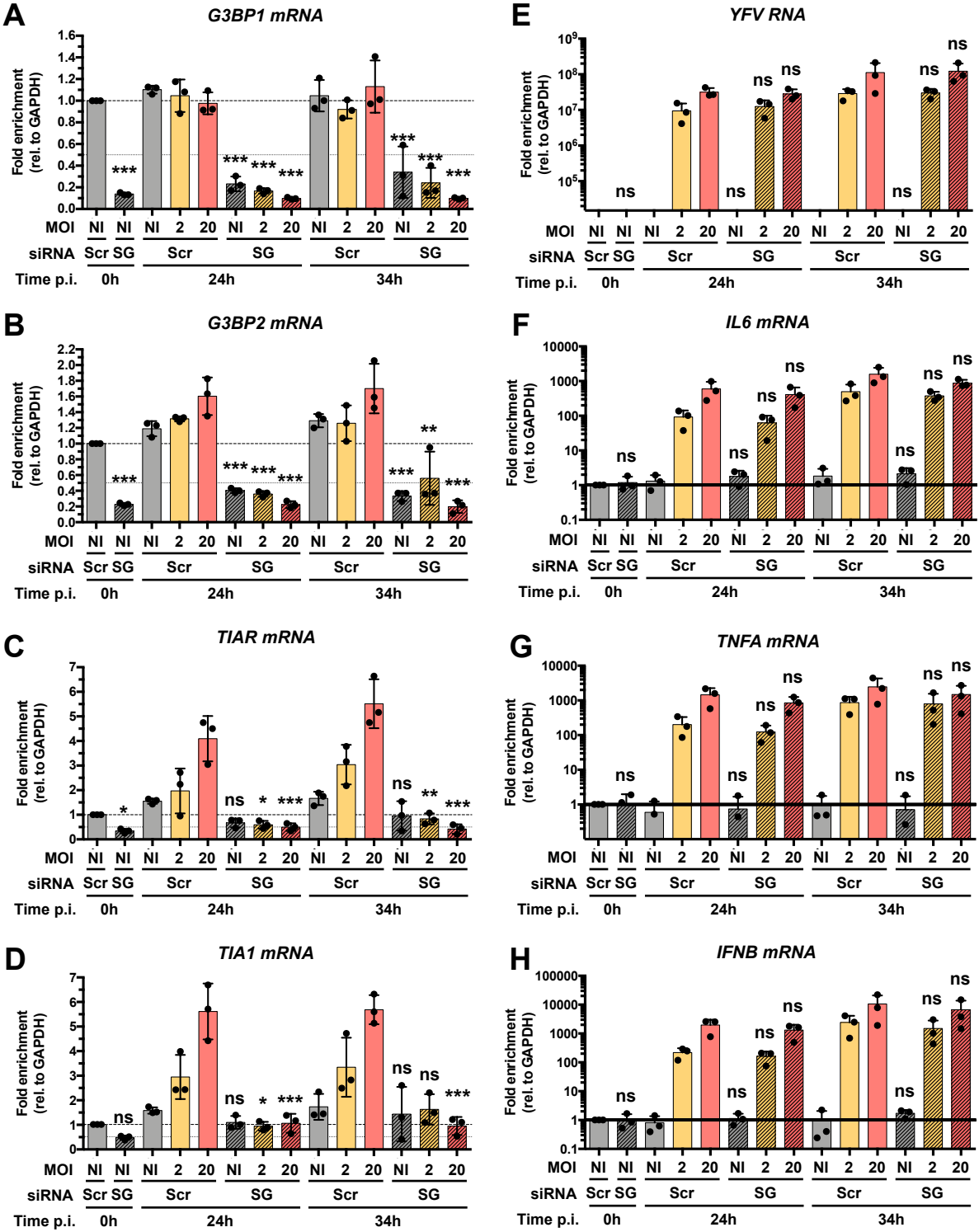
A
G3BP1 mRNA
B
G3BP2 mRNA
C
TIAR mRNA
D
TIA1 mRNA
E
YFV RNA
F
IL6 mRNA
G
TNFA mRNA
H
IFNB mRNA
Fold enrichment (rel. to GAPDH)
MOI NI NI NI 2 20 NI 2 20 NI 2 20 NI 2 20
siRNA Scr SG Scr SG Scr SG
Time p.i. 0h 24h 34h

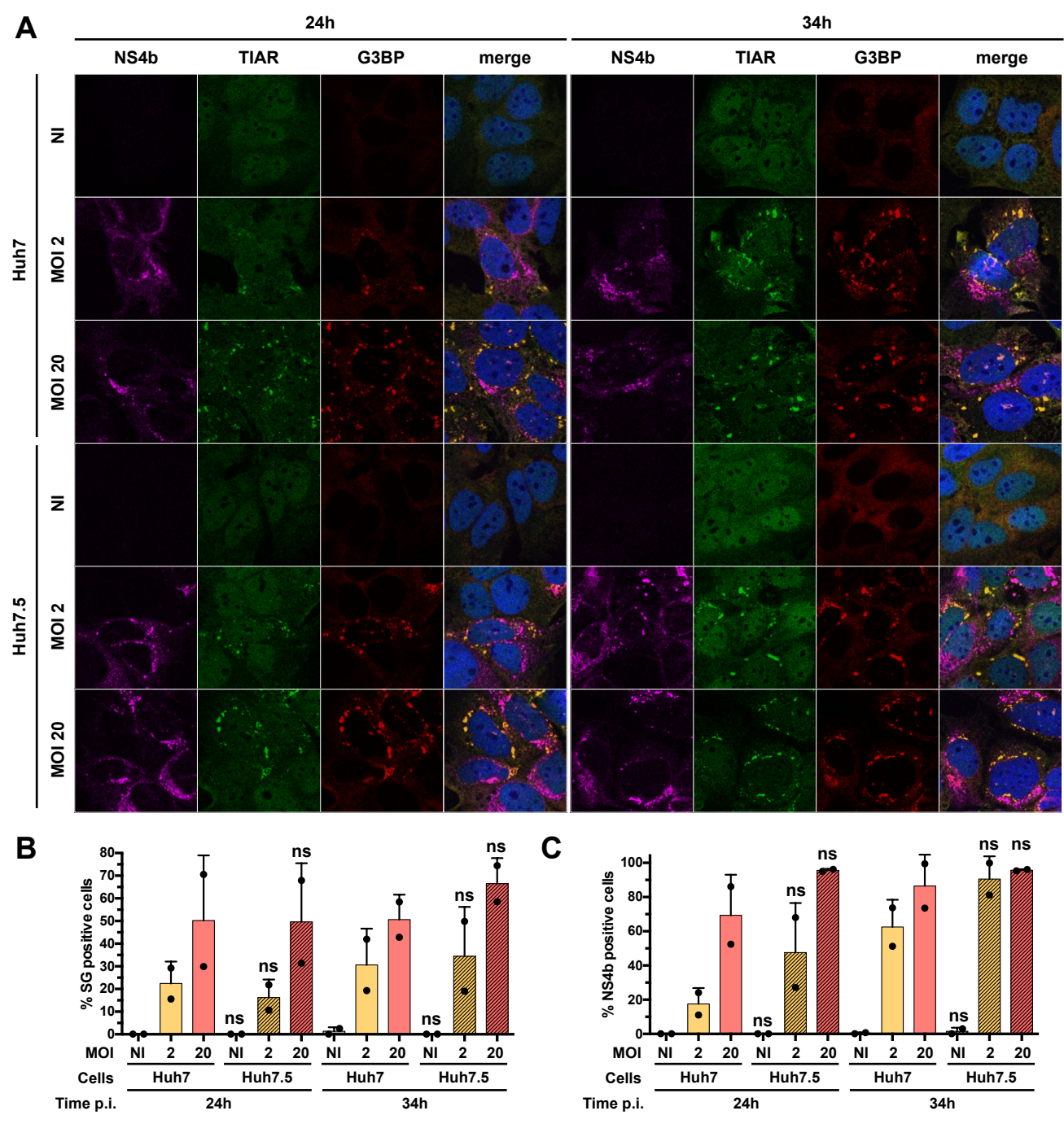
A
24h
34h
NS4b
TIAR
G3BP
merge
Huh7
Huh7.5
NI
MOI 2
MOI 20
B
% SG positive cells
ns
MOI
NI
2
20
Cells
Huh7
Huh7.5
Time p.i.
24h
34h
C
% NS4b positive cells

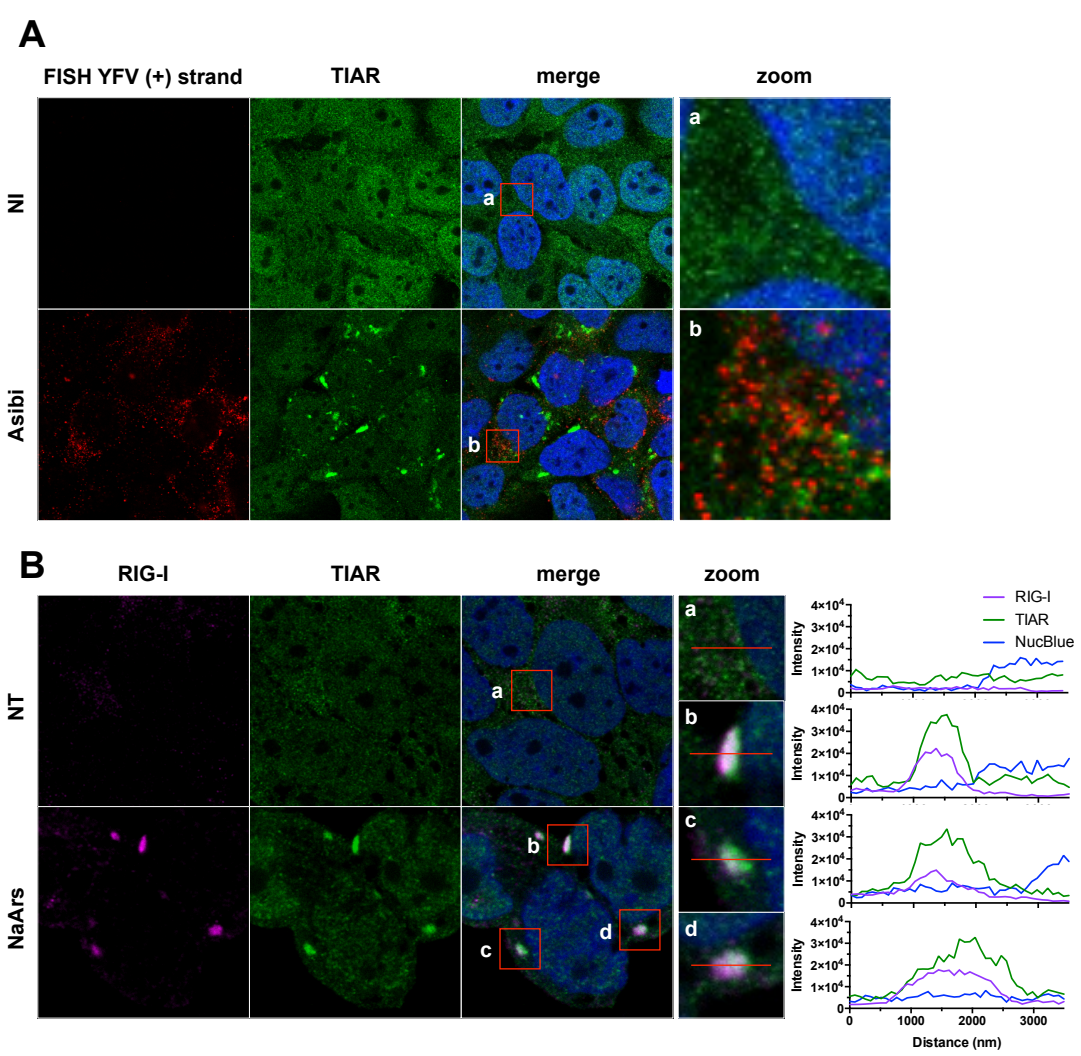
A
FISH YFV (+) strand
TIAR
merge
zoom
NI
Asibi
a
b
B
RIG-I
TIAR
merge
zoom
NT
NaArs
a
b
c
d
RIG-I
TIAR
NucBlue
Intensity
4×10⁴
3×10⁴
2×10⁴
1×10⁴
0
1000
2000
3000
Distance (nm)